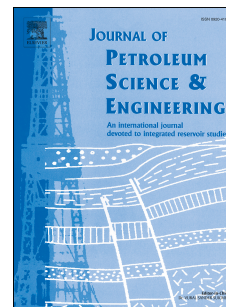


# Journal Pre-proof

Modelling the effects of reservoir parameters and rock mineralogy on wettability during low salinity waterflooding in sandstone reservoirs

Motaz Saeed, Prashant Jadhawar, Subhash C. Ayirala, Rockey Abhishek, Yingfang Zhou



PII: S0920-4105(22)00545-9

DOI: <https://doi.org/10.1016/j.petrol.2022.110676>

Reference: PETROL 110676

To appear in: *Journal of Petroleum Science and Engineering*

Received Date: 29 January 2022

Revised Date: 1 May 2022

Accepted Date: 19 May 2022

Please cite this article as: Saeed, M., Jadhawar, P., Ayirala, S.C., Abhishek, R., Zhou, Y., Modelling the effects of reservoir parameters and rock mineralogy on wettability during low salinity waterflooding in sandstone reservoirs, *Journal of Petroleum Science and Engineering* (2022), doi: <https://doi.org/10.1016/j.petrol.2022.110676>.

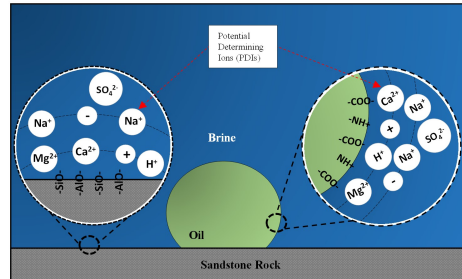
This is a PDF file of an article that has undergone enhancements after acceptance, such as the addition of a cover page and metadata, and formatting for readability, but it is not yet the definitive version of record. This version will undergo additional copyediting, typesetting and review before it is published in its final form, but we are providing this version to give early visibility of the article. Please note that, during the production process, errors may be discovered which could affect the content, and all legal disclaimers that apply to the journal pertain.

© 2022 Published by Elsevier B.V.

**CRedit Authorship Contribution Statement**

**Motaz Saeed:** Writing - original draft, Visualization, Investigation, Methodology, Software, Data curation, Formal Analysis. **Prashant Jadhawar:** Conceptualization, Visualization, Supervision, Formal Analysis, Writing - review & editing. **Subhash Ayirala** - Validation, Formal Analysis, review. **Rocky Abhishek:** Formal Analysis, review. **Yingfang Zhou:** co-supervision, review.

Journal Pre-proof



Journal Pre-proof

1       **Modelling the effects of reservoir parameters and rock mineralogy on**  
2       **wettability during low salinity waterflooding in sandstone reservoirs**

3  
4       Motaz Saeed<sup>a</sup>, Prashant Jadhawar<sup>a,\*</sup>, Subhash C. Ayirala<sup>b</sup>, Rockey Abhishek<sup>c</sup>,  
5       Yingfang Zhou<sup>a</sup>

6       <sup>a</sup> *School of Engineering, University of Aberdeen, Aberdeen AB24 3UE, Scotland, UK*

7       <sup>b</sup> *Upstream Advanced Research Center (EXPEC ARC), Saudi Aramco, Dhahran, Saudi Arabia*

8       <sup>c</sup> *Department of Energy and Petroleum Engineering, University of Stavanger, Stavanger, Norway*

9       **1 Abstract**

10       Low salinity waterflooding has been reported to yield incremental oil recovery from both field  
11       applications and laboratory experiments compared to regular waterflooding. Crude oil-brine-rock  
12       (COBR) interactions dictate wettability alteration during low salinity waterflooding in sandstones.

13       In this work, triple-layer surface complexation modelling (TLM) is utilised to simulate the  
14       interactions at rock-brine and oil-brine interfaces, while accommodating the crucial role of  
15       sandstone mineralogy in surface chemistry. Derjaguin-Landau-Verwey-Overbeek (DLVO) theory  
16       is applied to characterise the COBR stability. Moreover, we propose the use of the maximum  
17       energy barrier (MEB) parameter, which is calculated from the DLVO theory's interaction potential,  
18       as an indicator of reservoir wettability.

19       Correlating the MEB with the experimentally measured contact angles revealed an abrupt increase  
20       in contact angles as the MEB drops below the zero-value thereby leading to a less water-wet COBR  
21       system. Results analyses showed that the different clays affect the rock-brine zeta potential and  
22       wettability distinctly based on their surface site densities and specific surface areas. And the studied  
23       clays cause the zeta potential to become more negative in the order: smectite > montmorillonite >

24 illite > chlorite > kaolinite. Subsequently, further investigation employing the developed TLM and  
25 MEB revealed that higher amounts of kaolinite will make the reservoir more oil-wet.  
26 Lastly, the sensitivity analysis performed on reservoir wettability indicated that the ionic  
27 composition is the most important factor to affect rock wettability followed by pH and temperature.  
28 Moreover, the presence of  $\text{CaCl}_2$  salt in the formation water significantly suppresses the areas of  
29 strong water wettability under varying reservoir conditions compared to NaCl salt.  
30 The work conducted in this study presents a novel approach to model the individual and combined  
31 effects of sandstone minerals, specifically, quartz, kaolinite, chlorite, illite, montmorillonite and  
32 smectite, on the overall sandstone zeta potential behaviour. Furthermore, a new method was  
33 proposed to characterise reservoir wettability as a function of the maximum energy barrier which  
34 allowed us to obtain valuable insights into the most affecting reservoir parameters on COBR  
35 wettability. These findings will have practical implications to efficiently design the low salinity  
36 waterflooding processes for sandstone reservoir applications.

37 **Keywords:** *Rock-Brine Interface, Sandstone Reservoirs, Wettability Alteration, Triple-layer*  
38 *Surface Complexation Modelling, Low Salinity Waterflooding*

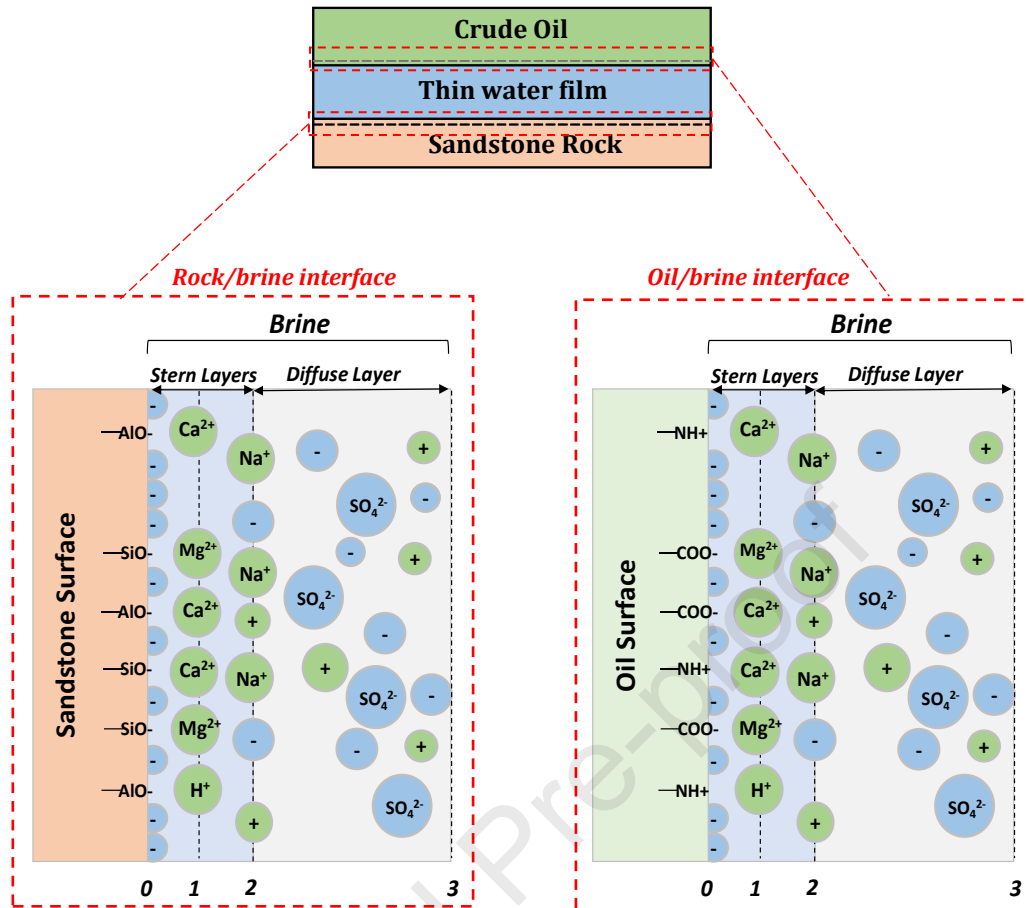
## 39 **2 Introduction**

40 Incremental oil recovery by low salinity waterflooding (LSWF) has been observed in both  
41 experimental and field applications in the sandstone porous media and has been the focus of  
42 numerous research studies [1]. LSWF has gained significant attention in the past two decades since  
43 it is relatively cheap when compared to other conventional enhanced oil recovery technologies  
44 (EOR) relying on costly chemicals and solvents. It also does not need major modifications in  
45 producing facilities besides capitalizing on the waterflooding infrastructure already available in  
46 sandstone oil fields. The synergization of LSWF with chemicals (surfactant, polymer) and  
47 nanoparticles is also recently becoming popular due to the favourable effects of low salinity water  
48 to reduce chemical usage and achieve higher oil recoveries [2-5].

49 Several mechanisms have been suggested to be the reason behind LSWF incremental recoveries  
50 including the fines migration, multi-component ion exchange (MIE), double-layer expansion, and  
51 alkaline-like effect [6-10]. There is no common consensus on a single mechanism, and it is also  
52 most likely that a combination of these mechanisms may be in play depending on studied systems  
53 and conditions. Double-layer expansion is widely believed to play an important role in bringing  
54 out the favourable low salinity effect on changing the wettability of the porous medium via the  
55 ionic interactions at the oil-brine and rock-brine interfaces. This paper presents the nano-scale  
56 results of such interactions using a newly developed triple-layer surface complexation model  
57 (TLM) in the crude oil-brine-rock system relevant to a sandstone reservoir. Wettability alteration  
58 from oil-wet to water-wet conditions is believed to be a result of the double-layer expansion [11].  
59 The charges at the oil-brine and rock-brine interfaces determine the thickness of thin water film  
60 between the oil and rock surfaces. Negative charges at both interfaces cause them to repulse,  
61 leading to the expansion of the thin water film thickness. Such expansion results in a more stable  
62 colloidal crude oil-brine-rock system in sandstones, where the rock surface is in more contact with  
63 brine than oil making the system water-wet. The interactions at the oil-brine and rock-brine  
64 interfaces depend on the brine composition as well as the surface-active functional groups at the  
65 oil and rock surfaces. The common surface-active groups on the oil surface are (-NH) and (-  
66 COOH), and on the sandstone rock surface are (>AlOH) and (>SiOH). These surface groups  
67 undergo protonation/deprotonation reactions and association/dissociation reactions with the  
68 potential determining ions (PDIs) present in the brine, which determines the oil and rock surface  
69 charges. More details on experimental evidence demonstrating how reservoir parameters dictate  
70 the COBR interactions and low salinity waterflooding performance in sandstone rocks can be found  
71 elsewhere [12].

72 Interactions at the oil-brine and rock-brine interfaces are simulated by the surface complexation  
73 models (SCM). Brady and Krumhansl [13] highlighted that diffuse double-layer (DDL) SCM can

74 be used to calculate the concentration of the electrostatic bridges connecting the oil and clay  
75 surfaces, thus predicting the degree of oil adhesion before and after the LSWF. The electrostatic  
76 bridges [13] are a result of a series of chemical reactions and electro-kinetic attraction forces. The  
77 COBR system in their model included rock containing kaolinite clay, oil with functional groups  
78 carboxylic (-COOH) and nitrogen bases (-NH<sup>+</sup>) and divalent cations Ca<sup>2+</sup> and Mg<sup>2+</sup> in water. They  
79 concluded that high concentrations of certain oppositely charged species such as [ $> \text{Al}:\text{Si}-\text{O}^-$ ], [ $>$   
80  $\text{Al}-\text{O}-\text{H}_2^+$ ], [-COOCa<sup>+</sup>], [-COO<sup>-</sup>], [-NH<sup>+</sup>] present on rock and oil surfaces, will lead to the  
81 electrostatic attraction between the two surfaces resulting in the adhesion of oil to rock surface  
82 (Figure 1). Details on the other oil-brine and rock-brine DDL-SCMs for both sandstone and  
83 carbonate rocks have been reported elsewhere [14-21].



84

85 **Figure 1 (top) Representation of thin water film between oil/brine and rock/brine interfaces,**  
 86 **(bottom) Representation of the sandstone-brine and oil-brine electrical interfacial layers**

87 On the other hand, triple-layer surface complexation models (TLMs) include three adsorption  
 88 layers rather than two layers which is the case in double-layer models (see Figure 1). The layers in  
 89 a TLM are the inner Helmholtz layer constrained by the electrostatic planes 0- and 1-planes, the  
 90 outer Helmholtz layer between the 1- and 2-planes and the diffuse layer extending from the 2-plane  
 91 to 3-plane. The inner and outer Helmholtz layers are known as the Stern layers as depicted in Figure  
 92 1. Moreover, TLM enables the modelling of inner and outer Helmholtz layer complexes and the  
 93 charge distribution of the adsorbed potential determining ions between the different electrostatic  
 94 planes leading to a better representation of the electrical interfacial layers [22-24]. A few triple-  
 95 layer surface complexation models (TLM) were developed to describe sandstone rock-brine  
 96 interfaces [25-31]. Most of these previous TLMs used single minerals such as quartz and kaolinite



97 to describe the rock surface. However, the other clay minerals such as illite, chlorite, smectite,  
98 montmorillonite, muscovite etc. are present in the sandstone and other clays. The individual and  
99 combined effect of these other minerals on the overall surface charge and zeta potential in  
100 sandstone rock systems were not accommodated in those investigated TLMs, which can be  
101 considered as the most important limitation of previously reported models in the existing  
102 knowledge.

103 The mineralogy of sandstone affects the wetting condition in the crude oil-brine-rock system  
104 [11,13]. The sandstone rock surface chemistry is the resultant of the protonation/deprotonation and  
105 cation/anion sorption reactions of the mineral surface groups. The clay surface charge can be  
106 defined as the sum of the edge plane and basal plane charges. In this work, we consider only the  
107 edge plane charge which is controlled mainly by the surface groups Aluminol ( $>AlOH$ ) and Silanol  
108 ( $>SiOH$ ). In addition to the surface groups, clay surface charge is also dictated by the clay specific  
109 surface area, temperature, brine salinity and pH [13,32]. Different clay minerals such as kaolinite,  
110 illite and chlorite have different surface group site densities and specific surface areas. These  
111 differences result in distinct surface charge behaviour for the individual clays and their overall  
112 contribution to the sandstone rock surface charge [33,34].

113 In the present study, we build upon our findings from a previously published work [35] utilising  
114 the newly developed oil-brine TLM, by integrating it with the sandstone-brine interfacial TLM  
115 (this work) to evaluate the effect of different clay minerals. These clay minerals include kaolinite,  
116 illite, chlorite, montmorillonite and smectite (in addition to quartz), which represent a considerable  
117 portion of the overall sandstone rock mineralogy [36]. The values of the  $>AlOH$  and  $>SiOH$  surface  
118 site densities and clay specific area for the modelled sandstone minerals were extracted from  
119 various published experimental and modelling studies, as summarised in Table 1.

120 The novelty of work undertaken in this investigation lies in (i) the inclusion of the individual and  
121 combined effects of different reservoir minerals, specifically quartz, kaolinite, chlorite, illite,

122 montmorillonite and smectite, on the surface charge behaviour at sandstone surface and (ii)  
 123 development of the correlation between the maximum energy barrier, (defined as the maximum of  
 124 the DLVO theory's interaction potential energy curve [37]) contact angles and reservoir wettability  
 125 in different crude oil-brine-sandstone rock systems.

126 The following section will present the methodology adopted in this work. Subsequently, the results  
 127 of sandstone-brine interface model validation and zeta potential sensitivity analysis are discussed.  
 128 Later, wettability correlation with the maximum energy barrier parameter is presented followed by  
 129 sensitivity analysis of COBR wettability to various reservoir parameters.

130 **Table 1 Specific surface area and surface site density for sandstone minerals modelled in this work**

Mineral	Specific surface area (g/m <sup>2</sup> )		Surface site density (site/nm <sup>2</sup> )		
	Value	Reference	>AlOH	>SiOH	Reference
Kaolinite	12	[38]	5.5	5.5	[33,38]
Chlorite	2.4	[38]	5.5	5.5	This study
Illite	22.3	[39]	≈2.6	≈5.3	[34]
Montmorillonite	71	[38]	≈1	≈2	[40]
Smectite	31	[41]	≈0.6	≈0.6	[41]
Quartz	0.426	[42]	-	10	[43]

### 131 **3 Methodology**

132 The methodology adopted to develop the triple-layer surface complexation model describing the  
 133 sandstone-brine interfacial interactions is presented. The developed sandstone-brine TLM was then  
 134 validated and employed to assess the impact of rock mineralogy, salinity, and pH on the rock-brine  
 135 zeta potential. The validated sandstone-brine interface model is further integrated with our  
 136 previously reported oil-brine TLM [35] and the Derjaguin, Landau, Verwey, and Overbeek  
 137 (DLVO) theory [44] to understand film stability and reservoir wettability alteration during the  
 138 LSWF.

### 139 **3.1 Sandstone Rock-Brine Triple-Layer Surface Complexation Model (TLM)**

140 A sandstone rock-brine TLM was developed using the Donnan approach in CD-MUSIC, a module  
141 of the geochemical code PHREEQC<sup>TM</sup> [45]. This TLM simulates the interactions at the rock-brine  
142 interface while taking account of the following parameters: inner and outer-Helmholtz layer  
143 capacitances, protonation/deprotonation and association/dissociation reactions equilibrium  
144 constants, surface site densities, specific surface areas and charge distribution. The assumptions  
145 made during this TLM development were: (i) quartz, kaolinite, illite, chlorite, montmorillonite and  
146 smectite are the most abundant minerals in the sandstone reservoir, hence their individual  
147 behaviour governs the overall sandstone surface charge behaviour; (ii) the overall average  
148 behaviour can be predicted by weight-averaging the specific surface area and surface site densities  
149 for each mineral; and (iii) the surface site density of chlorite is same as kaolinite due to a lack of  
150 data in the published literature. The results obtained from triple-layer modelling were validated  
151 against the reported experimental data (see Table 2) available in the literature.

152 **Table 2 Summary of experimental conditions used for the published zeta potential data**  
 153 **at the sandstone-brine interface**

Reference	Rock Sample	Brine Electrolyte	Brine Salinity	pH	Temperature (°C)
[46]	Berea Sandstone	NaCl, CaCl <sub>2</sub>	1500 ppm	2 to 11	25
[47]	Sandstone	NaCl, CaCl <sub>2</sub> , MgCl <sub>2</sub>	0.1 - 5 wt.%	7.3 to 9	25
[48]	Kaolinite, Montmorillonite	NaCl, CaCl <sub>2</sub>	0.05 - 0.3 wt%	6.05 to 6.83	Room Temperature
[49]	Kaolinite	CaCl <sub>2</sub> , MgCl <sub>2</sub>	50 - 500 mmol/L	1.8 to 7.8	25
[50]	Sandstone	NaCl	0.2 - 10 wt.%	7.1 to 8.4	65
[51]	Berea Sandstone, Scioto Sandstone	Deionized Water, Aquifer Water, Seawater	5,436 - 174,156 mg/L	7.29 to 7.84	25
[52]	Kaolinite	NaCl	0.02 mol/L	3 to 11	25
[53]	Kaolinite	NaCl	0.0001 - 0.01 mol/L	3 to 11	25

154  
 155 The surface groups of minerals used are Aluminol (>AlOH) and Silanol (>SiOH). The potential  
 156 determining ions (PDIs) modelled in the brine are calcium, magnesium, sodium, hydroxyl and  
 157 hydrogen ions. The effect of sulphate ions in brine on zeta potential at the rock-brine interface is  
 158 also evaluated in the model. The sodium ion forms an outer-sphere complex with the surface groups  
 159 (>Al:SiOH) with its charge distributed between the 1- and 2-planes, while the calcium and  
 160 magnesium ions form inner-sphere complexes with (>Al:SiOH) and have their charges on the 1-  
 161 plane [23,54].  
 162 For pure individual clay minerals, the values of specific surface areas and surface site densities for  
 163 >Al:SiOH, reported in Table 1, were directly used in the model to evaluate the rock-brine  
 164 interactions. In modelling the surface of a sandstone rock comprising multiple minerals, the

165 weighted-average values of the surface site densities and specific surface area were employed. The  
 166 specific surface area ( $SSA_{avg}$ ) used in the model was averaged by the mineral weight/volume % in  
 167 the overall sandstone rock mineralogy as shown in Eq. (1)

$$SSA_{avg} = \sum_i SSA_i \times wt_i\%(or\ vol_i\%) \quad \text{Eq. 1}$$

168 where  $SSA$  is the specific surface area and  $i$  denotes the mineral type. The surface site densities  
 169 ( $N_s$ ) for  $>AlOH$  and  $>SiOH$  were averaged based on both mineral weight/volume % in the overall  
 170 sandstone rock mineralogy and the specific surface area of each mineral, using the following  
 171 equation:

$$N_{s,avg} = \frac{\sum_i N_{s,i} \times SSA_i \times wt_i\%(or\ vol_i\%)}{SSA_{avg}} \quad \text{Eq. 2}$$

172 The capacitances (see Table 3) of the inner and outer Helmholtz layers determine the potential drop  
 173 across the layer. These are dependent on the dielectric constant of the electrolyte and the distance  
 174 between the planes. The detailed procedure for calculating the capacitance for each layer can be  
 175 found in Saeed et al. [35]. The thickness of the diffuse layer was assumed to be twice the screening  
 176 Debye length [34]. The inverse Debye length is calculated as follows:

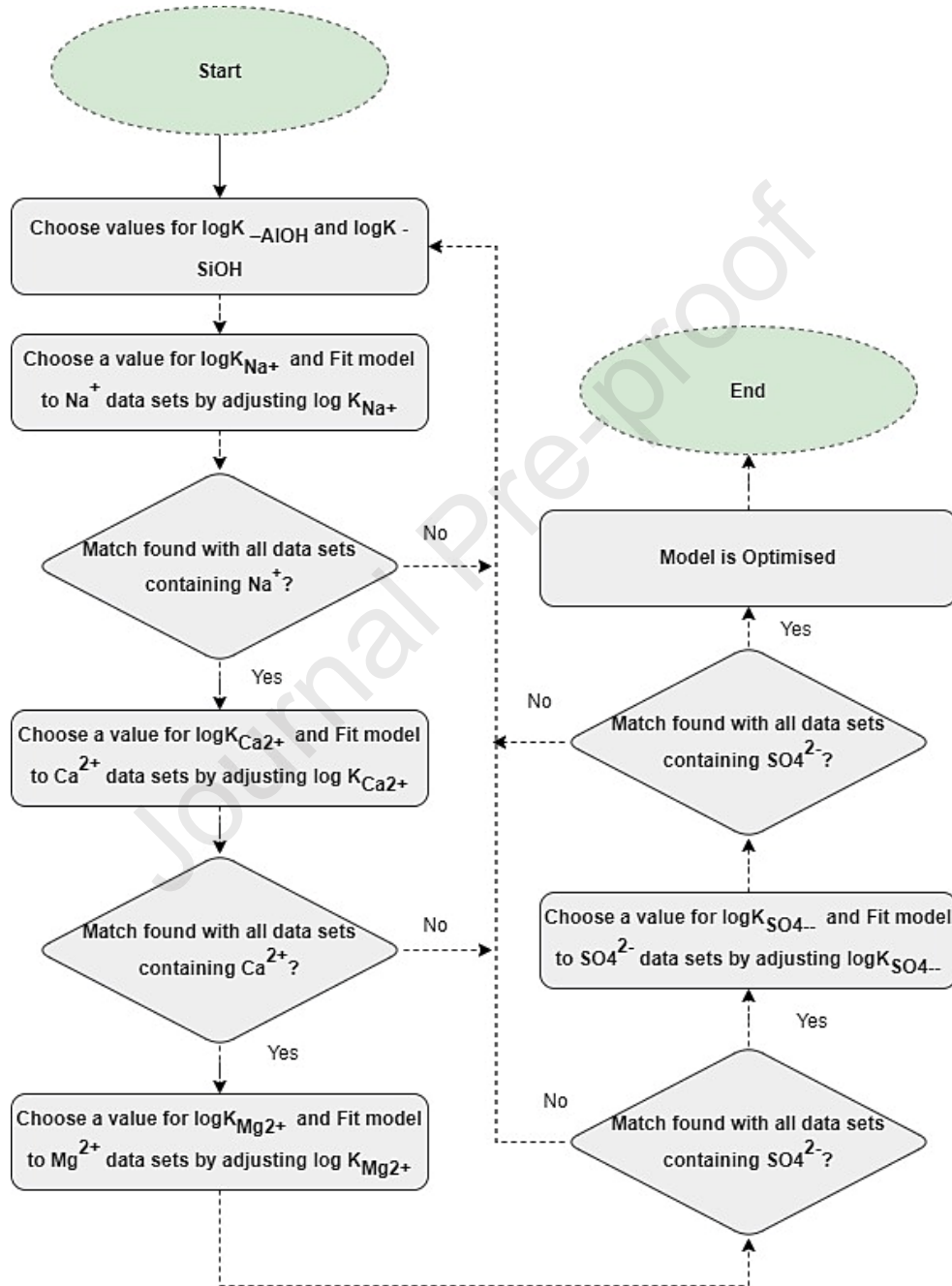
$$k^{-1} = \sqrt{\frac{\epsilon_o \epsilon_r k_B T}{2000 N_A e^2 I}} \quad \text{Eq. 3}$$

177 where  $k_B$  is the Boltzmann constant,  $T$  is the absolute temperature,  $N_A$  is Avogadro's number,  $e$  is  
 178 the electron charge, and  $I$  is the ionic strength of the solution.

### 179 3.1.1 Optimization of the sandstone Rock-Brine TLM

180 The association/disassociation equilibrium constants of the surface groups,  $>AlOH$  and  $>SiOH$ ,  
 181 were optimized to converge between the modelling and experimental zeta potential values. The  
 182 modelling optimization process, illustrated in Figure 2, follows the optimization process described  
 183 by Saeed et al. [35]. The experimental data required for the modelling run are brine composition,  
 184 pH, temperature and sandstone rock mineralogy to calculate the average specific surface area for

185 the rock and average surface site densities of  $>AlOH$  and  $>SiOH$ . The optimized surface  
 186 complexation reactions constants are shown in Table 3 along with the reactions' enthalpy, the  
 187 charge distribution of the modelled PDIs and the capacitances of the inner and outer Helmholtz  
 188 layers.



189  
 190  
 191 **Figure 2 Sandstone rock-brine TLM optimization process flowchart**

192

193 **Table 3 Association/disassociation equilibrium constants, charge distribution and capacitance values**  
 194 **optimised in this study for the developed sandstone-brine TLM**

Surface Complexation Reaction	Log K @ 25° C	Enthalpy (kJ/mol)	Charge Distribution			C <sub>1</sub> (F/m <sup>2</sup> )	C <sub>2</sub> (F/m <sup>2</sup> )
			0-plane	1-plane	2-plane		
$>AlOH + H^+ \leftrightarrow >AlOH_2^+$	0.8	-5	+1	0	0	2.57	2.57
$>AlOH \leftrightarrow >AlO^- + H^+$	-7.5	-40	-1	0	0	2.57	2.57
$>AlOH + Na^+ \leftrightarrow >AlONa + H^+$	-4.5	-60	-1	+0.5	+0.5	2.57	2.57
$>AlOH + Ca^{2+} \leftrightarrow >AlOCa^+ + H^+$	-3.5	-50	-1	+2	0	3.54	2.57
$>AlOH + Mg^{2+} \leftrightarrow >AlOMg^+ + H^+$	-3.5	-50	-1	+2	0	4.92	2.57
$>AlOH + SO_4^{2-} \leftrightarrow >AlO^- + HSO_4^-$	-1.5	-	-1	0	0	2.57	2.57
$>SiOH \leftrightarrow >SiO^- + H^+$	-6.5	-40	-1	0	0	2.57	2.57
$>SiOH + Na^+ \leftrightarrow >SiONa + H^+$	-2	-60	-1	+0.5	+0.5	2.57	2.57
$>SiOH + Ca^{2+} \leftrightarrow >SiOCa^+ + H^+$	-2.5	-50	-1	+2	0	3.54	2.57
$>SiOH + Mg^{2+} \leftrightarrow >SiOMg^+ + H^+$	-2.8	-50	-1	+2	0	4.92	2.57
$>SiOH + SO_4^{2-} \leftrightarrow >SiO^- + HSO_4^-$	-1.5	-	-1	0	0	2.57	2.57

195

196 The sandstone-brine TLM developed in this study overcomes the limitations of previously reported  
 197 sandstone rock-brine SCMs and TLMs [25-31]. The developed TLM successfully incorporates the  
 198 individual and combined effects of the most abundant clays and minerals present in sandstone  
 199 rocks, thereby providing an improved ability to quantify the impact of each clay on the overall zeta  
 200 potential and reservoir wettability. The model was found to be effective in describing the adsorption  
 201 of various PDIs i.e. H<sup>+</sup>, Na<sup>+</sup>, Ca<sup>2+</sup> and Mg<sup>2+</sup>, on the inner and outer Helmholtz layers of the  
 202 sandstone rock-brine interface. The model also describes the effect of sulphate ions present in brine  
 203 on the sandstone rock-brine interface.

### 204 3.2 Oil-brine interface TLM

205 Our previously reported oil-brine TLM [35] is integrated with the sandstone-brine TLM developed  
 206 in this study, to evaluate the complete Crude Oil Brine Rock (COBR) system. The stability of the  
 207 COBR was characterised using the DLVO theory calculations. The association/disassociation  
 208 reaction equilibrium constants, charge distribution and capacitance were also considered in this  
 209 study. The oil-brine TLM incorporates the effects of both the acidic and basic groups i.e. (-COOH)  
 210 and (-NH), on the oil surface, and the adsorption/desorption of the PDIs, Na<sup>+</sup>, Ca<sup>2+</sup>, Mg<sup>2+</sup> and H<sup>+</sup>,  
 211 on the oil surface groups. More details on the adopted oil-brine TLM can be found in [35].

### 212 3.3 Disjoining Pressure Calculations and Film Stability

213 The crude oil-brine-rock (COBR) system is analysed by calculating the disjoining pressure using  
 214 the DLVO theory. The calculation of disjoining pressure requires the knowledge of zeta potentials  
 215 at the oil-brine and rock-brine interfaces. These zeta potential values are adapted from the  
 216 simulation output of the developed TLM and the geochemical code PHREEQC. The disjoining  
 217 pressure can be calculated as the sum of two repulsive forces and an attractive force. The two  
 218 repulsive forces are the electrical double-layer force and the structural force, while the attractive  
 219 force is the Van der Waals force. To calculate the disjoining pressure, the individual forces are  
 220 calculated and added together to find the net force acting between the oil-brine and rock-brine  
 221 interfaces.

$$\Pi(h) = \Pi_{vdw}(h) + \Pi_{structural}(h) + \Pi_{electric}(h) \quad Eq 4$$

222 The Van der Waals forces between two plates including the retardation effects are calculated  
 223 according to the following formula [55]:

$$\Pi_{vdw}(h) = -\frac{A \left(15.96 \left(\frac{h}{\lambda_{lw}}\right) + 2\right)}{12\pi h^3 \left(1 + 5.32 \left(\frac{h}{\lambda_{lw}}\right)\right)^2} \quad Eq 5$$



224 where,  $\lambda_{lw}$  is the London wavelength and is assumed to be 100 nm [55],  $h$  is the distance between  
 225 the two interfaces and  $A$  is the Hamaker constant, obtained through [44]:

$$A = A_{v=0}(\kappa h)\exp(-2\kappa h) + A_{v>0} \quad Eq 6$$

226 where  $\kappa$  is the Debye-Huckel parameter,  $A_{v=0}$  and  $A_{v>0}$  are the contributions to Hamaker constant  
 227 at zero and finite frequencies, respectively obtained using the following equations [44]:

$$A_{v=0} = \frac{3}{4} kT \left( \frac{\varepsilon_1 - \varepsilon_3}{\varepsilon_1 + \varepsilon_3} \right) \left( \frac{\varepsilon_2 - \varepsilon_3}{\varepsilon_2 + \varepsilon_3} \right) \quad Eq 7$$

$$A_{v>0} \approx \frac{3h\nu_e}{8\sqrt{2}} \frac{(n_1^2 - n_3^2)(n_2^2 - n_3^2)}{(n_1^2 + n_3^2)^{0.5}(n_2^2 + n_3^2)^{0.5}\{(n_1^2 + n_3^2)^{0.5} + (n_2^2 + n_3^2)^{0.5}\}} \quad Eq 8$$

228  
 229 where  $\varepsilon_1$ ,  $\varepsilon_2$  and  $\varepsilon_3$  are the dielectric constants for medium 1, 2 and 3, as considered in our case for  
 230 hydrocarbons, quartz and water, respectively.  $n_1$ ,  $n_2$  and  $n_3$  are the refractive indexes for medium  
 231 1, 2 and 3, respectively. The values for these parameters to calculate the Hamaker constant can be  
 232 found in [44]. The structural forces are effective at low separation distances between the two  
 233 interfaces  $< 5$ nm [56] and are calculated as follows:

$$\Pi_{structural}(h) = A_s e^{-\frac{h}{h_s}} \quad Eq 9$$

234 where  $A_s$  is a coefficient, assumed to be  $1.5 \times 10^{10}$  Pa [37] and  $h_s$  is the characteristic length,  
 235 assigned the value of 0.05 nm [37].

236 For the two charged surfaces approaching each other, the two solutions for the Poisson-Boltzmann  
 237 equation can be obtained using two different conditions [37,55,57]. One solution is the constant  
 238 potential solution, and the other is the constant capacitance charge. It is predicted that a solution  
 239 between them occurs. In this work, it is assumed that a constant potential solution [58] applies to  
 240 simplify our calculations. Hence, the force resulting from the interaction of the two charged  
 241 surfaces of oil and sandstone can be calculated by

$$\Pi_{electric}(h) = n_b k_b T \left( \frac{2\psi_{r1}\psi_{r2} \cosh(\kappa h) - \psi_{r1}^2 - \psi_{r2}^2}{[\sinh(\kappa h)]^2} \right) \quad Eq 10$$

242 where  $n_b$  is the ion density in the bulk solution,  $k_b$  is the Boltzmann constant ( $1.38 \times 10^{-23} \text{J/K}$ ),  $\psi_{r1}$   
 243 and  $\psi_{r2}$  are the reduced surface potentials for the rock-brine and oil-brine interfaces, respectively,  
 244 and  $\kappa$  is the Debye-Hückel reciprocal length. The reduced potential can be calculated as follows:

$$\psi_r = \frac{ze\zeta}{kT} \quad Eq 11$$

245 where  $\zeta$  is the zeta potential at the interface of interest. The specific interaction potential energy  
 246 between two phases interacting through a third phase can be calculated as follows [37]

$$\omega = \int_h^{h_{eq}} (\Pi - \Pi_{eq}) \cdot dh \quad Eq 12$$

247 where  $h_{eq}$  and  $\Pi_{eq}$  are the separation distance and disjoining pressure at equilibrium conditions. The  
 248 stability of the COBR system is directly related to the maximum interaction potential energy barrier  
 249 (MEB), below which the VdW forces become dominant and the colloid falls into an unstable region  
 250 and is destroyed [559].

251 In this work, we propose the use of MEB as the main indicator for film stability, and hence the  
 252 wettability of the reservoir under investigation. The maximum energy barrier is calculated as the  
 253 maximum of the interaction potential curve. To understand the effects of various reservoir  
 254 parameters on the oil-brine-sandstone rock system's stability and wettability, the MEB is evaluated  
 255 for several cases by varying the studied reservoir parameters. The MEB is calculated at zero  
 256 capillary pressure in all the studied cases. Capillary pressure does affect the reservoir's wettability,  
 257 however, setting its value to zero eliminates its effects on wettability and therefore focuses the  
 258 investigation on the basis of brine, oil and rock compositions, pH and temperature only. For this  
 259 application, we observe that the maximum energy barrier for the modelled cases ranges at film  
 260 thicknesses between 0.5 and 1.5 nm. Hence, for consistency, we calculate the maximum of the  
 261 interaction potential at this range for all the studied cases. With a higher MEB, the oil-brine-

262 sandstone system is more stable, and thus more water wet. As the MEB decreases, the stability of  
263 the oil-brine-sandstone system becomes less stable and less water-wet. The factors affecting the  
264 oil-brine-sandstone system's wettability include pH, temperature, salinity, oil TAN and TBN, and  
265 rock mineralogy among others. The first step in calculating the interaction potential energy is to  
266 model the oil-brine and rock-brine zeta potentials. The disjoining pressure is calculated according  
267 to *Eq 4*. Interaction potential is calculated using *Eq 12*. Finally, sensitivity analysis was utilised to  
268 evaluate the sensitivity of COBR wettability to changes in oil TAN and TBN, sandstone rock's  
269 average rock site density, brine composition, pH and temperature. This eventually enabled us to  
270 produce wettability maps for NaCl and CaCl<sub>2</sub> systems to further understand the importance of each  
271 parameter on wettability determination during the low salinity waterflooding process in sandstone  
272 reservoirs.

## 273 **4 Results and Discussion**

274 The published data sets of zeta potential measurements using brines and sandstone rock (see Table  
275 2) were first extracted and then used to calibrate and validate the developed triple-layer model  
276 (TLM). The extracted datasets composed of experimental results performed under varying brines,  
277 sandstone mineralogical composition, pH, and temperatures. The correlation analysis between the  
278 calculated MEB and experimentally measured contact angles was performed. Results of sensitivity  
279 analysis are reported and discussed to evaluate the importance of the various parameters in dictating  
280 the zeta potential of a sandstone-brine interface and the sandstone reservoir wettability.

### 281 **4.1 Sandstone-brine Triple-layer Model Validation**

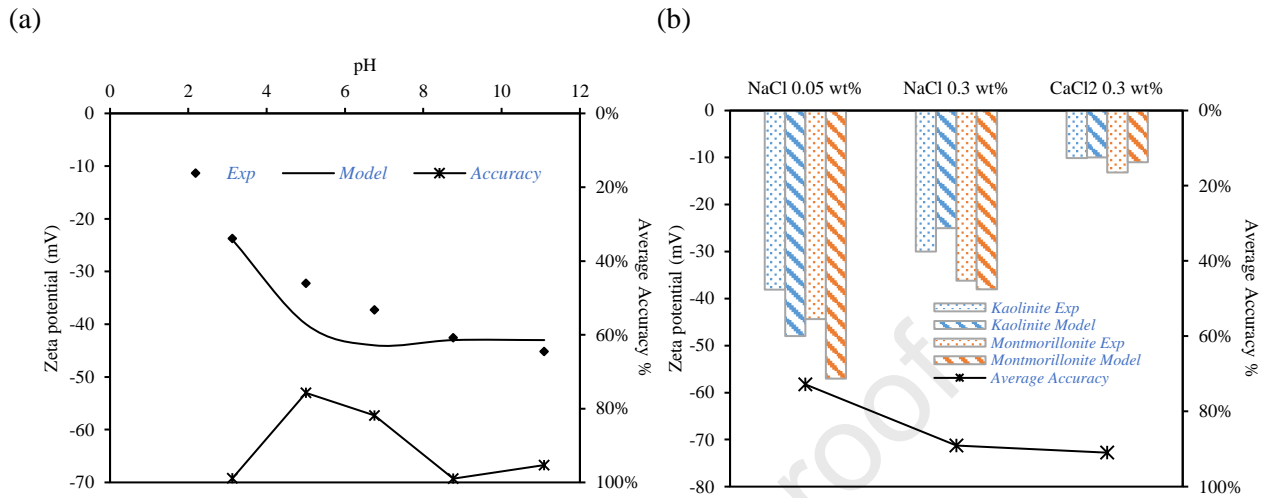
282 The developed model is validated, against the experimental datasets as detailed in Table 2. The  
283 validation was carried out by comparing the experimentally measured zeta potential with the  
284 model-predicted zeta potential values.

#### 285 4.1.1 Modelling the zeta potential of pure clays

286 The experimental data from Yukselen-Aksoy and Kaya [52] were used to validate and calibrate the  
287 model developed in this work. Yukselen-Aksoy and Kaya used kaolinite as the rock sample and  
288 NaCl as the background electrolyte with a concentration of 0.02 M NaCl. The zeta potential was  
289 predicted for a pH range of 3 to 11 and at 25 °C temperature. The TLM simulation results (Figure  
290 3) display the capability of the model to predict the trend of the zeta potential change with pH in  
291 the studied range. The results indicate that an increase in the pH value leads to higher negative zeta  
292 potential values which can be attributed to the enhancement of Al:SiOH deprotonation. This  
293 deprotonation causes the increase of the negatively charged Al:SiO<sup>-</sup> surface groups which  
294 progressively charge the kaolinite surface with a negative charge. The values of zeta potential  
295 calculated by the TLM were in close agreement with the experimental values except at pH between  
296 5.0-6.8 where discrepancies are apparent, and the accuracy of the model drops to the range 76% -  
297 82% which highlights some slight inaccuracy in modelling.

298 The effect of NaCl and CaCl<sub>2</sub> electrolyte on the zeta potential at the pure clay-brine surface was  
299 evaluated in this study using the experimental data extracted from Bazyari et al. [48]. The TLM  
300 was used to predict the zeta potential values at the rock-brine interface for two different types of  
301 pure clay minerals - kaolinite and montmorillonite. The TLM predicted results are matched with  
302 the experimental results reported [48] (see Figure 3). The model was able to closely predict the zeta  
303 potential values. It can also be seen that CaCl<sub>2</sub> electrolytes caused the zeta potential to be less  
304 positive for both kaolinite and montmorillonite in contrast to the NaCl electrolyte effect. This is  
305 attributed to the presence of the divalent cation Ca<sup>2+</sup> which causes higher electrical screening to the  
306 negative charge present on the clay surfaces. The model shows accuracy ranging between 73% and  
307 91% for the studied cases. The model exhibits better accuracy in predicting zeta potential in higher  
308 ionic strength electrolytes. This can be explained by the fact that higher ionic strength leads to

309 suppressing the zeta potential values, thereby minimising the discrepancies between model and  
 310 measured zeta potentials.



311  
 312 **Figure 3 Experimental and modelling zeta potential values for (Left) Kaolinite [52] and (Right)**  
 313 **kaolinite and montmorillonite [53]**

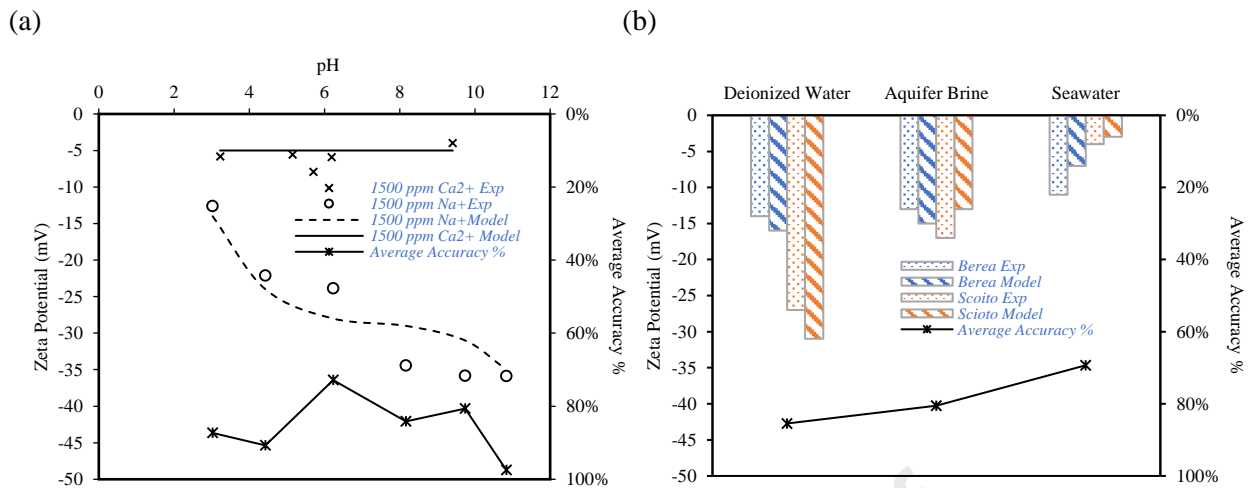
#### 314 4.1.2 Modelling the zeta potential of sandstone rocks

315 The rock-brine TLM proposed in our work was also used to replicate the experimental results of  
 316 Farooq et al. [46] who studied the effect of varying cationic valences and pH conditions on an  
 317 outcrop Berea sandstone sample. All their experiments were conducted at 25°C temperature  
 318 conditions. The Berea sandstone sample mineralogy was used to calculate the rock properties  
 319 required as input parameters of the TLM: average >Al:SiOH site density and average specific  
 320 surface area using Eq. 1 and Eq. 2. Then the model was run to predict the zeta potential of the two  
 321 cases using 1500 ppm and 1500 ppm electrolyte concentrations of NaCl and CaCl<sub>2</sub>, respectively.  
 322 The capacitance of the first layer parameter was varied according to the type of electrolyte used,  
 323 2.57 and 3.54 F/m<sup>2</sup> for NaCl and CaCl<sub>2</sub> in that order. For all cases, the second layer capacitance  
 324 was fixed at a value of 2.57 F/m<sup>2</sup>.

325 The model results and their comparison with the experimentally reported zeta potentials are shown  
 326 in Figure 4a. The model successfully predicts the zeta potential for the Berea sandstone sample

327 within close proximity in both NaCl and CaCl<sub>2</sub> electrolytes. In addition, the model also provided  
328 accurate zeta potential predictions at high and low pH values with only small discrepancies at  
329 higher pH values. The model accuracy ranged between the average 73% and 97% averaged for  
330 both electrolytes containing Na<sup>+</sup> and Ca<sup>2+</sup> respectively.

331 The developed sandstone-brine model was also tested against its ability to capture the effect of  
332 various clays present in the sandstone rock sample. Alotaibi et al. [51] focused on using Berea and  
333 Scioto sandstone samples in different electrolytes including deionized water, aquifer water and  
334 seawater. The salinity of the different electrolytes in addition to the mineralogy of the two rock  
335 samples were used in the developed model to calculate the zeta potential. Figure 4b presents both  
336 the experimental and modelling results as calculated from the TLM. The results demonstrate the  
337 ability of the model to give an accurate prediction of the zeta potential for both Berea and Scioto  
338 sandstone (Figure 4b) in deionized water and aquifer water with accuracies of 85% and 81%,  
339 respectively. However, there is distortion in modelling the seawater experiments which can be  
340 attributed to its considerably higher concentration of ions, and the different types of ions that are  
341 not included in this model. This has led the model to have a lower accuracy of about 70%. It is  
342 expected that incorporating the adsorption of more ions on the inner and outer Helmholtz layers  
343 would increase the model accuracy, especially in such cases where seawater is used as an  
344 electrolyte.

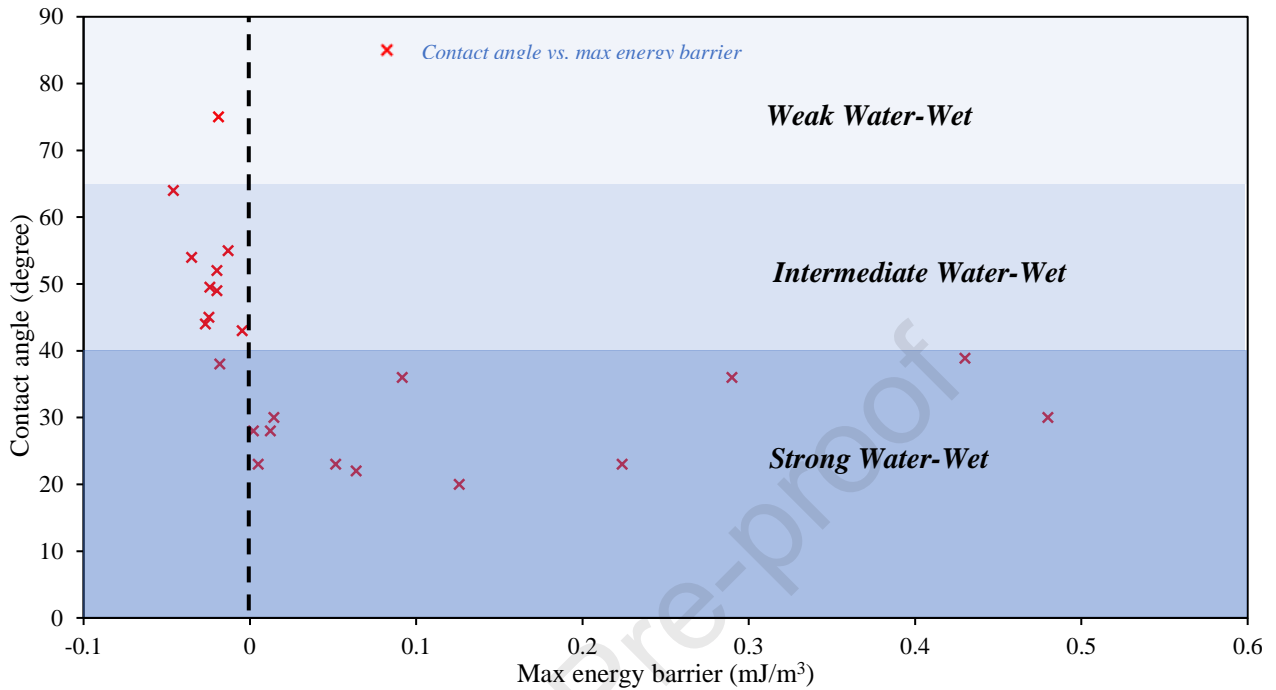


345  
346 **Figure 4 Experimental and modelling zeta potential values for (a) Berea sandstone [46] and (b)**  
347 **Berea sandstone sample and Scioto sandstone sample [51]**

#### 348 4.2 Wettability, film stability and the maximum energy barrier

349 First, we test the hypothesis that the maximum energy barrier is an indicator of reservoir wettability.  
350 The maximum of the interaction potential curve was calculated for several published experimental  
351 datasets [11, 17, 50, 59 – 61] obtained using different sandstone samples, reservoir minerals, oil  
352 composition, brine composition and temperature conditions. The MEB values was calculated from  
353 the zeta potential measurements reported in these published experimental datasets. The results were  
354 then fitted with the measured contact angles, as shown in Figure 5. Reservoir wettability is defined  
355 by the contact angle with the range 0° to 40° being strong water-wet, 40° to 65° as intermediate  
356 water-wet and 65° to 90° as weak water-wet. Figure 5 shows that as the MEB decreases from 0.07  
357 to zero, the contact angle increases from 20° to 32°. However, this increase in the contact angle is  
358 sharper when MEB goes into negative. Such observation indicates that a small reduction in the  
359 MEB below zero-value increases the contact angle sharply, thereby causing the system to become  
360 less water wet (intermediate water-wet). The data depicted in Figure 5 clearly show two trends, one  
361 below zero MEB where the reservoir wettability abruptly becomes weaker with the decrease in the

362 MEB. While above zero MEB, the reservoir tends to stay in the strong water-wet region. These  
 363 results validate our hypothesis that the MEB can be used as an indicator of reservoir wettability.



364

365 **Figure 5 Correlation between experimentally measured contact angles and calculated maximum**  
 366 **energy barrier for each contact angle [11, 17, 50, 59 – 61]**

### 367 4.3 Effect of clay minerals on zeta potential and maximum energy barrier

368 Using the optimized modelling parameters of the different clay minerals shown in Table 1 and  
 369 Table 3, the model was further employed to understand and compare the effects of the individual  
 370 clay minerals on zeta potential at the rock-brine interface. The model was run for each individual  
 371 clay under the same conditions. The zeta potential curve for the five clay minerals under study is  
 372 plotted against the system pH (Figure 6). The results show that smectite, montmorillonite and  
 373 chlorite result in more negative zeta potential values with smectite having the highest negative zeta  
 374 potential within the studied conditions. The effect of kaolinite on zeta potential is lower compared  
 375 to the other three clays. Similar trend is observed for both 0.05 M NaCl (Figure 6a) and 0.005 M  
 376 NaCl (Figure 6b) electrolytes. The order by which the clays affect the zeta potential is directly  
 377 correlated with the site density of the surface species at clays. From Table 1, the site density at



378 >Al:SiOH surface for kaolinite and smectite is 11 site/nm<sup>2</sup> and 1.2 site/nm<sup>2</sup> respectively. If we  
379 compare the zeta potential curves for kaolinite and smectite in Figure 6, it is evident that in the case  
380 of kaolinite the zeta potential values are less negative than those of the smectite case. This can be  
381 attributed to the higher presence of >Al:SiOH sites on the kaolinite mineral compared to smectite,  
382 leading to a more negatively charged >Al:SiO<sup>-</sup>. These are the possible sites where the positively  
383 charged Na<sup>+</sup> can adsorb to. This adsorption leads to the screening of the surface charge present on  
384 the clay surface. Hence, the higher the presence of clay minerals in the sandstone rock, especially  
385 kaolinite, the more the zeta potential values at the sandstone rock-brine interface tend to be less  
386 negative. The experimental results published in [38,48] are in line with our findings. Mahani et al.  
387 [62] also highlighted that clays act as pinning points to crude oil which supports the results obtained  
388 in this study. Montmorillonite clay exhibited higher negative zeta potential values in comparison  
389 with kaolinite clay. Other studies [47,63,64] reported that the montmorillonite clay had higher  
390 negative zeta potential than kaolinite, illite and chlorite in electrolytes with different ionic strengths  
391 and over a wide range of pH. Our finding that the montmorillonite clay leads to negative zeta  
392 potential values higher than kaolinite, chlorite and illite also agrees with the published experimental  
393 results. Da Costa et al [65] measured the zeta potential for three types of sandstone: Botucatu, Berea  
394 and Bentheimer, in various electrolyte ionic strengths. Zeta potential curve shifted towards more  
395 negative values as the clay content in the sandstone rock decreased. Hence, the Bentheimer  
396 sandstone had a zeta potential curve that is more negative than the Berea sandstone, which is more  
397 negative than the Botucatu sample, exemplifying an important role of clays, as concluded in our  
398 work.

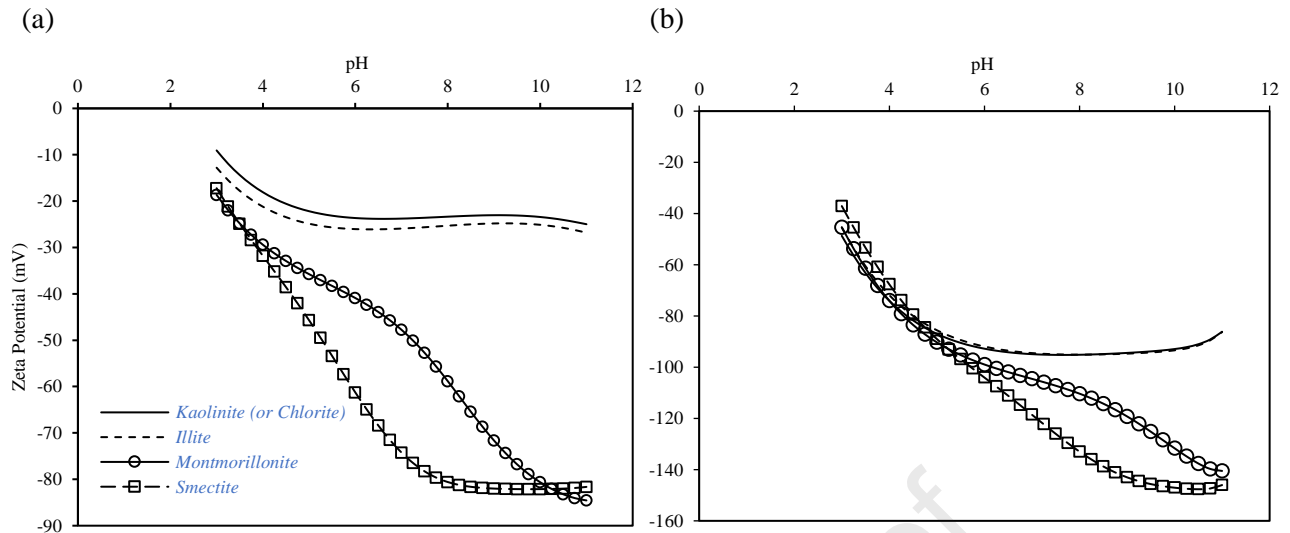


**Figure 6 Zeta potential curves for different clay minerals in (a) 0.05 M NaCl electrolyte and (b) 0.005 M NaCl electrolyte**

399

400

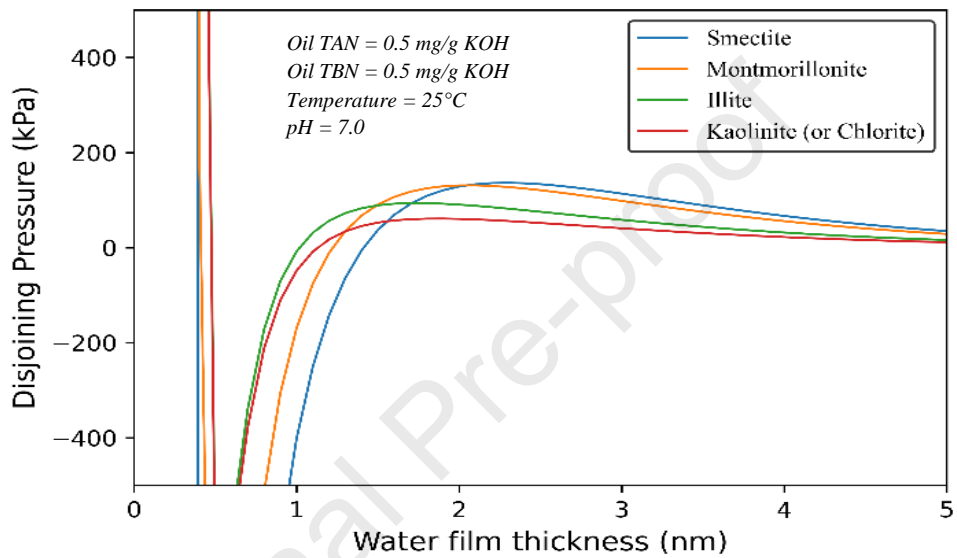
401

402 The  $>Al:SiOH$  surface site densities used are the averaged  $>AlOH$  and  $>SiOH$  site densities based  
 403 on the mineral contents of the sandstone rock in question. The average  $>Al:SiOH$  surface site  
 404 density affects the overall stability of the COBR system via the zeta potential at the rock-brine  
 405 interface. More the negatively charged  $>Al:SiO^-$ , higher will be the site density (where the cations  
 406 can adsorb to), hence a less negative zeta potential at the rock-brine interface. This will lead to a  
 407 lower overall disjoining pressure and interaction potential as shown in Figure 7. The results  
 408 depicted in Figure 7 are in line with the findings of Bazyari et al [48] to confirm that  
 409 montmorillonite exhibits disjoining pressure higher than kaolinite for several background  
 410 electrolytes over a wide range of water film thickness. Based on these analyses and the MEB  
 411 calculated for each clay (see Figure 8), it is concluded that the clays investigated in this study cause  
 412 the zeta potential to be more negative and hence the COBR system more stable in the following  
 413 order: smectite  $>$  montmorillonite  $>$  illite  $>$  chlorite  $>$  kaolinite. This implies that the higher the  
 414 presence of clays that have higher  $>Al:SiOH$  site density such as kaolinite, the lower the stability  
 415 of the COBR system. Borysenko et al. [66] measured the air/water contact angles of kaolinite and  
 416 montmorillonite. They found that the montmorillonite clays had lower contact angles than kaolinite

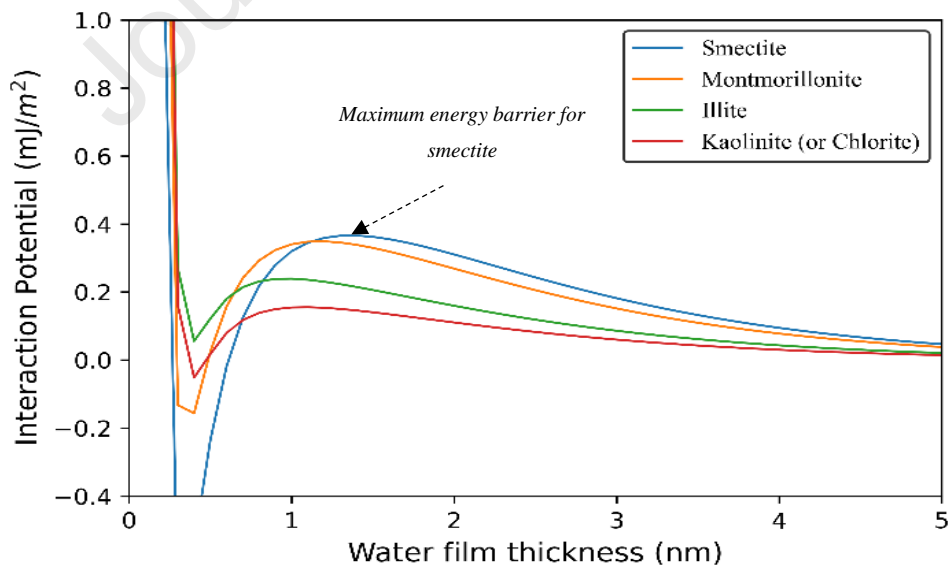
417 clays, which is in line with the MEB results depicted in Figure 8. The rapid change in the maximum  
 418 energy curve with the average rock site density demonstrates the significance of the sandstone rock  
 419 mineralogy in dictating the wettability of the oil-brine-rock system.

420

(a)

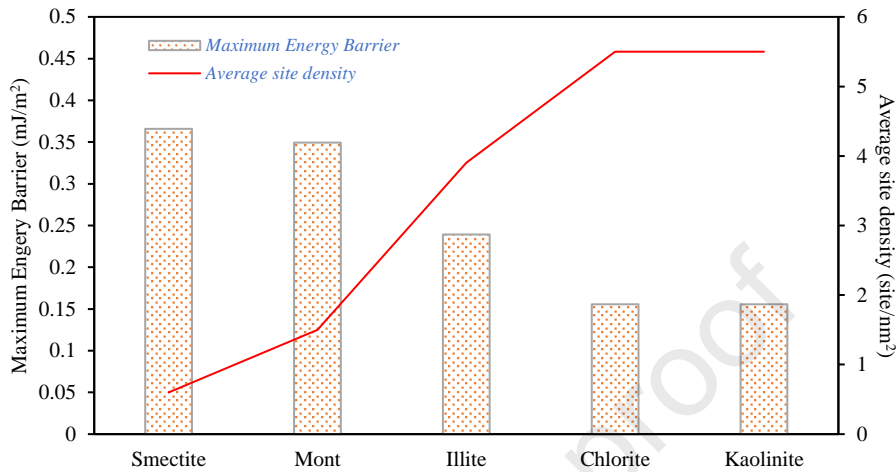


(b)



421

422 **Figure 7 (a) Disjoining pressure and (b) interaction potential curves for oil-brine and rock-brine**  
 423 **interfaces with various clay minerals**



424  
 425 **Figure 8 Maximum energy barrier variation with clay mineral type and average rock site density**

#### 426 4.4 Sensitivity of energy barrier to reservoir conditions and composition

427 Sensitivity analyses were performed to understand the contribution of various parameters in the  
 428 overall stability and wettability of the COBR system. These sensitivity analyses were carried out  
 429 using the workflow developed in this study, including predicting the zeta potential values using the  
 430 developed TLMs followed by calculating the disjoining pressure and interaction potential energy  
 431 for each studied case. Finally, the MEB was determined from the calculated interaction potential  
 432 energy curves. The studied parameters include brine ionic strength, pH, temperature, rock  
 433 mineralogy, oil TAN and oil TBN. The analysis was carried out by determining a base case value  
 434 for each parameter, as well as minimum and maximum values to simulate the reservoir conditions  
 435 of potential interest (see Table 4). Then each parameter was allowed to be changed in isolation  
 436 from the other parameters between its minimum and maximum values, which allowed us to  
 437 quantify the individual impact of each parameter within the studied range. The results of the  
 438 sensitivity analyses are presented in Figure 9. From Figure 9, it can be clearly seen that the most  
 439 important parameters that affect the reservoir wettability are the ionic strength, pH, and reservoir

440 temperature followed by the rock site density. This specific finding highlights that injection water  
 441 salinity is a key parameter to governing the prospects of low salinity waterflooding in sandstone  
 442 reservoirs. Analysis shows that increasing the salinity from 0.1 to 3 M NaCl will result in the MEB  
 443 reversing its sign from positive to negative, hence, shifting reservoir wettability from strong water-  
 444 wet to weak or intermediate water-wet conditions. The results of these analyses also highlight the  
 445 importance of rock mineralogy in dictating the overall reservoir wettability. By increasing the  
 446 average rock site density from the base value 2.5 site/nm<sup>2</sup> to the maximum of 5.5 site/nm<sup>2</sup>, which  
 447 corresponds to the kaolinite clay site density (see Table 1), the film stability drastically drops 53%  
 448 from its base value 0.47 mJ/m<sup>2</sup>. Such finding indicates that the inclusion of mineralogy is essential  
 449 in sandstone reservoir wettability prediction. Another interesting finding in our work is that the  
 450 effect of oil composition change on the overall system stability is not as pronounced as the other  
 451 parameters. Results show that changing the TAN of crude oil between a maximum and minimum  
 452 of 0.01 and 3 mg KOH/g results in a maximum of 31% change in the energy barrier. While  
 453 changing the TBN of a crude oil between 0 and 3 mg KOH/g results in a minimal less than 1% in  
 454 the energy barrier. This observation suggests that the amounts of acidic polar compounds in the  
 455 crude oil have a dominant effect over basic components to impact the wettability in sandstones.

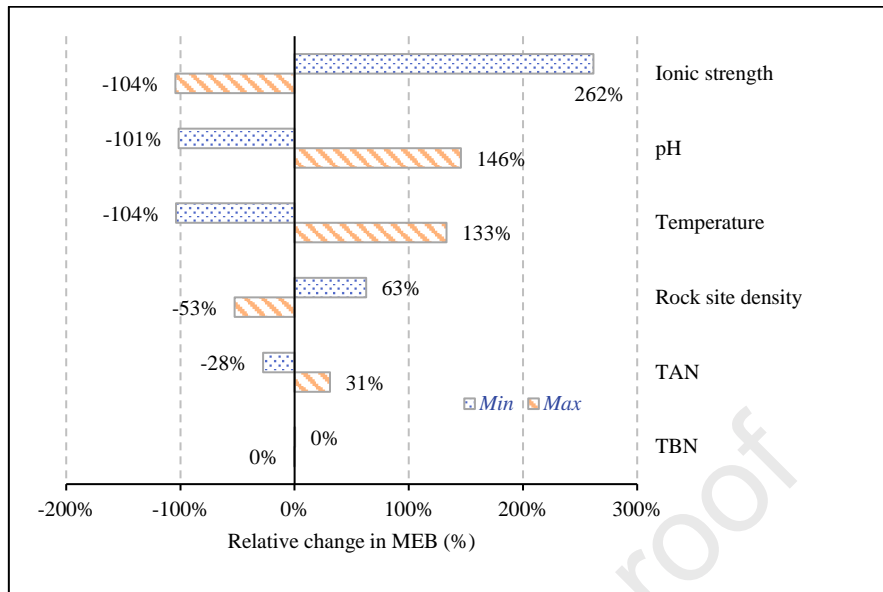
456 **Table 4 Ranges of the selected parameters for sensitivity analyses**

Parameter	Base	Min	Max	Maximum energy barrier (mJ/m <sup>2</sup> )		
				Base	Min	Max
<b>Ionic strength (M NaCl)</b>	0.5	0.01	3	0.47	1.7	-0.02
<b>pH</b>	7	5	9	0.47	-0.0068	1.154
<b>Temperature (°C)</b>	60	25	100	0.47	-0.018	1.095
<b>Rock site density (site/nm<sup>2</sup>)</b>	5	1.2	11	0.47	0.764	0.223
<b>TAN (mg KOH/g)</b>	0.5	0.01	3	0.47	0.34	0.616
<b>TBN (mg KOH/g)</b>	0.5	0	3	0.47	0.472	0.469

457

458 We further employed our triple-layer model to evaluate the effect of continuous change of the  
459 studied parameters on the overall oil-brine-sandstone system. Figure 10 compares the effects of  
460 temperature and pH changes on the MEB using the base case values listed in Table 4. It can be  
461 observed the increase in pH value results in a continuous increase in the energy barrier almost in a  
462 linear manner (Figure 10a), which allows us to predict that an increase in pH will always result in  
463 strengthening the water-wet conditions in sandstone reservoirs. This is one of the suggested  
464 mechanisms of the low salinity waterflooding [7] which is also the underlying mechanism in  
465 alkaline flooding. Figure 10b shows that an increase in the temperature between 25 and 100 °C, in  
466 cases of using 0.5 and 1 M NaCl, results in an increase in the energy barrier from -0.02 mJ/m<sup>2</sup> to  
467 0.53 mJ/m<sup>2</sup> and 1.0975 mJ/m<sup>2</sup>, respectively. However, in the case of a 0.01 M NaCl background  
468 electrolyte, the energy barrier increases from 0.695 mJ/m<sup>2</sup> to a maximum 1.75 mJ/m<sup>2</sup> at 80 °C  
469 before dropping slightly to 1.6 mJ/m<sup>2</sup> at 100 °C. These results indicate that the pronounced effect  
470 of temperature on reservoir wettability in low salinity waterflooding mostly takes place below 80  
471 °C. It can also be concluded that the temperature increase beyond 80 °C - 100 °C may result in  
472 reversing the wettability trend into less favourable conditions. This trend could be due to possible  
473 surface overcharging, leading to a decrease in the negative surface charge and eventually reversing  
474 the wettability [67].

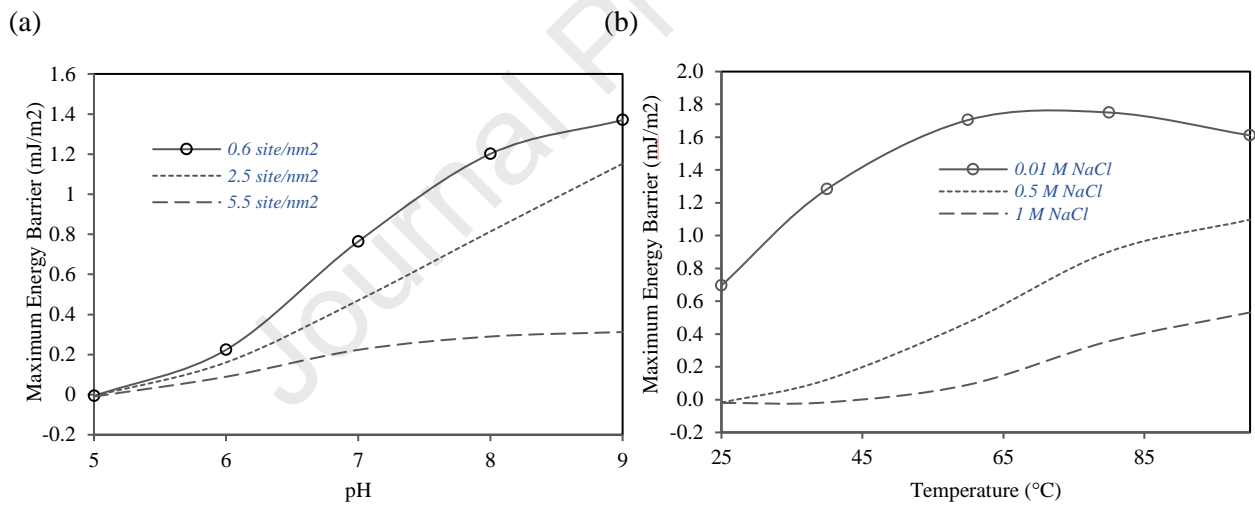
475



476

477

**Figure 9** Relative change of maximum energy barrier against the different parameters



478

479

480

**Figure 10** Sensitivity of maximum energy barrier against (a) pH at various average rock site densities and (b) temperature at various salinities

481

482

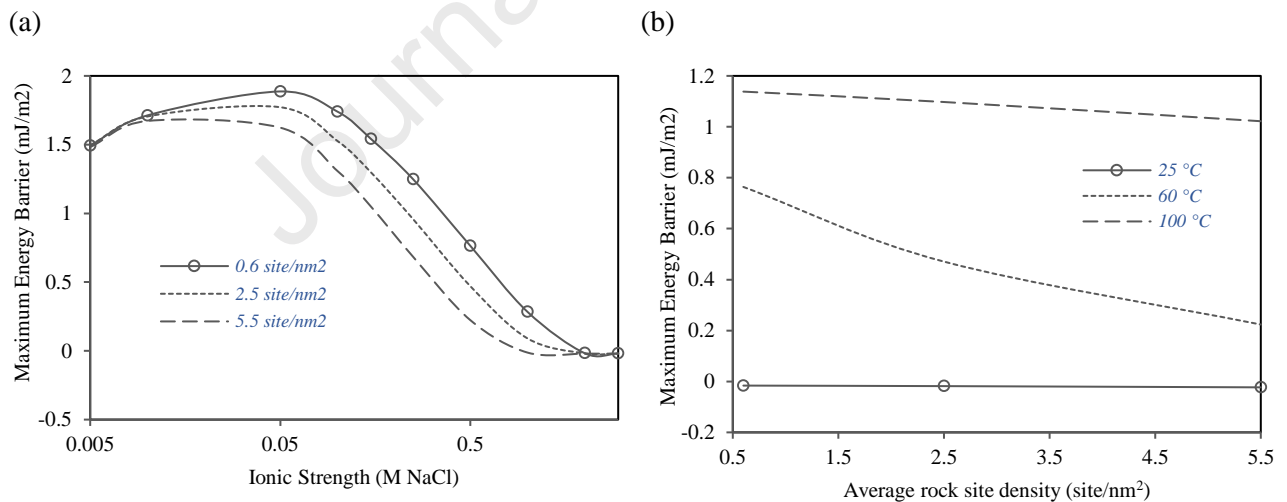
483

484

485

The effects of the ionic strength and average rock site density on the MEB were calculated and the results are shown in Figure 11. It shows that the increase in ionic strength of NaCl from 0.005 M to 3 M at different rock site densities results in a reduction in the MEB. It can be noticed that the effect of ionic strength on the MEB is pronounced in the range between 0.05 and 2 M NaCl where the MEB drops from 1.77 to  $-0.02 \text{ mJ/m}^2$ . The energy barrier drops below the zero value when the

486 ionic strength increases beyond 2 M NaCl and stabilises at a maximum negative value of  
 487 approximately  $-0.02 \text{ mJ/m}^2$ . This implies that the target of low salinity waterflooding in a case  
 488 where a reservoir with the initial conditions such as shown in Table 4 and formation water of 2 M  
 489 NaCl, would be to use the injection water with a salinity less than 1 M NaCl for observing the  
 490 favorable effect. Figure 11b also shows that the increase in the average rock site density has a  
 491 descending effect on the oil-brine-sandstone system which is specifically evident at temperatures  
 492 higher than  $25^\circ\text{C}$ . A high average rock site density results in more sites being available for the  
 493 cations present in the brine to adsorb and screen the negative charge present on the sandstone  
 494 surface. Such less negative charge results in less repulsion between the rock surface and the  
 495 negatively charged oil surface leading to more oil adherence to the rock surface. This is evident  
 496 quantitatively in Figure 11b for the case of  $60^\circ\text{C}$  temperature where the increase of average rock  
 497 site density from  $0.6$  to  $5.5 \text{ site/nm}^2$  leads to a drop in the MEB from  $0.764 \text{ mJ/m}^2$  to  $0.224 \text{ mJ/m}^2$ ,  
 498 shifting the wettability towards less water-wet conditions.

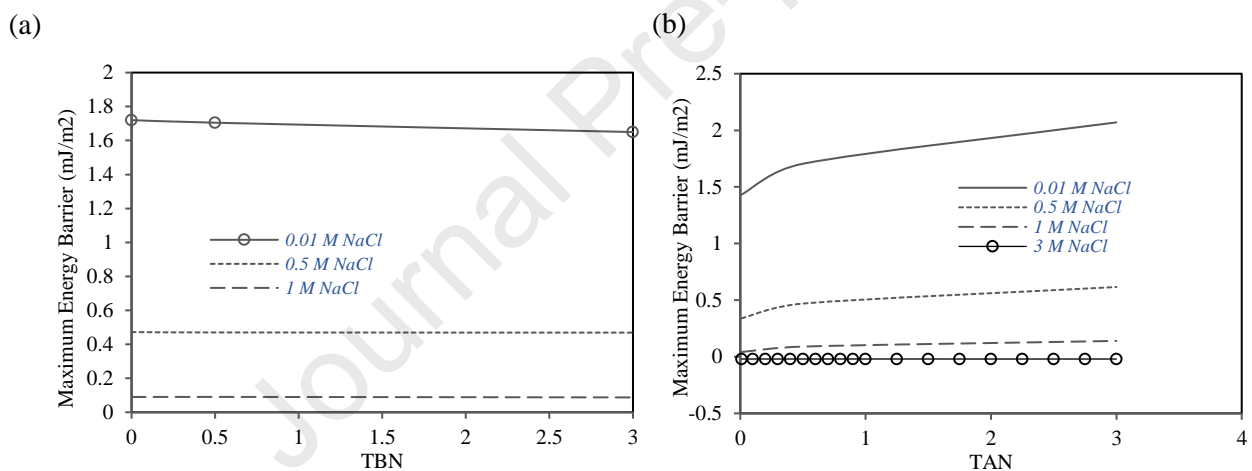


499  
 500 **Figure 11 Sensitivity of maximum energy barrier against (a) ionic strength at various average rock**  
 501 **site densities and (b) average rock site density at various temperatures**

502 The impact of oil polar compounds on the MEB are depicted in Figure 12. It can clearly be seen  
 503 that the effect of TAN on the MEB is more pronounced compared to TBN. This can be attributed  
 504 to the fact that the TBN and positively charged amines surface groups are more present at lower



505 pH values where an excess of hydrogen ions associates with (-NH) to create (-NH<sub>2</sub><sup>+</sup>). And because  
 506 our studied range of pH is between 5 and 9, the effects of TBN and positively charged amine groups  
 507 are not fully captured. Nevertheless, we can assume that the oil TBN does not have a pronounced  
 508 effect under the usual reservoir conditions. TAN on the other hand does influence the oil-brine-  
 509 sandstone system stability and wettability in reservoir conditions. Figure 12b shows that at lower  
 510 salinities, an increase in the TAN results in an increase in the MEB. However, as the salinity  
 511 increases and the concentration of the positive sodium ions available for adsorption increases, the  
 512 increase in TAN results in a negligible change in the MEB. NaCl salinities above 1 M NaCl show  
 513 a reversal in the trend where increasing the TAN leads to a very slight decrease in the MEB and  
 514 hence the system stability.



515  
 516 **Figure 12 Sensitivity of maximum energy barrier against (a) TBN and (b) TAN at various salinities**

#### 517 4.5 Wettability change with reservoir conditions

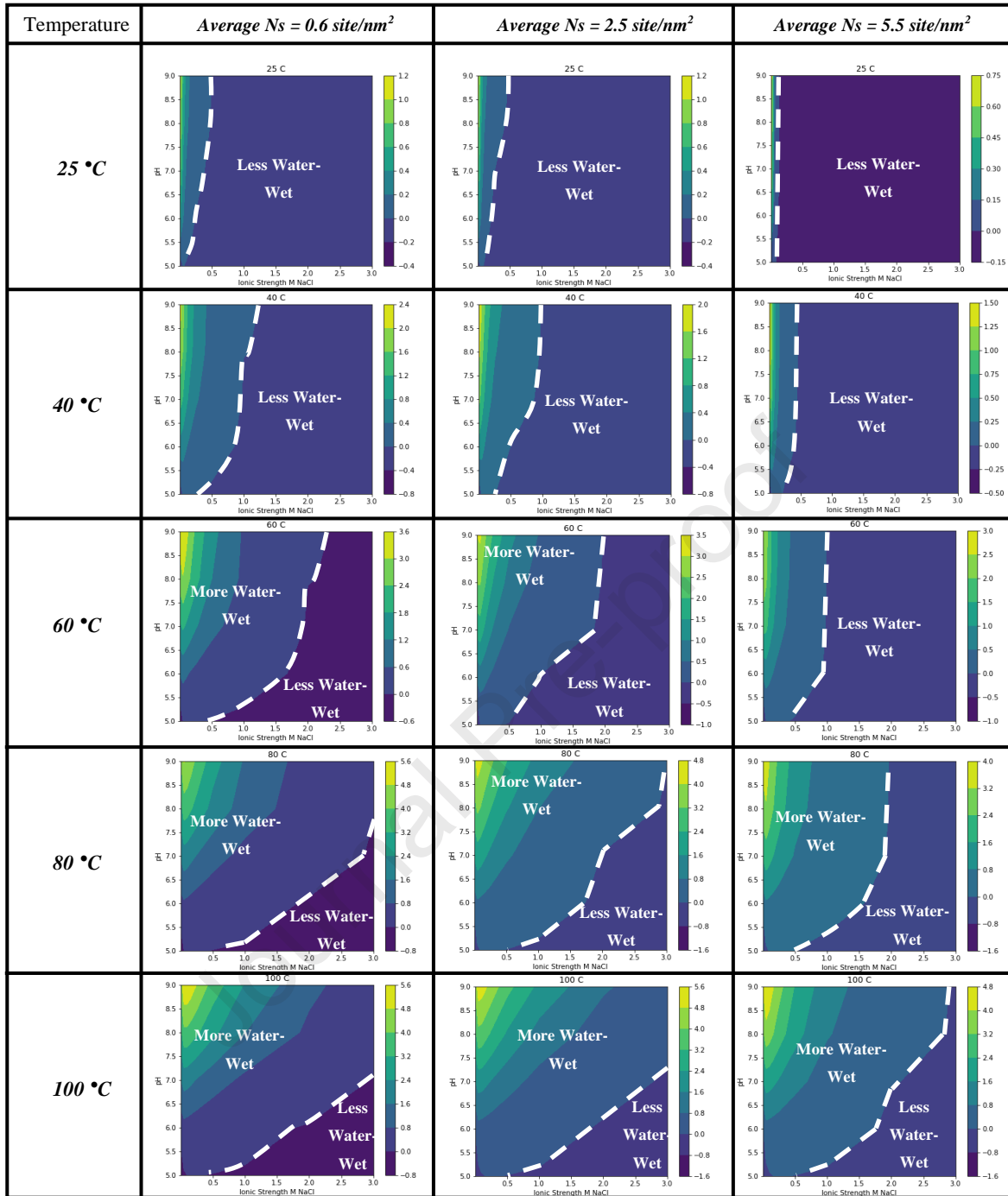
518 In this section, the approaches used in this study are combined to quantify and provide an indicative  
 519 adhesion or wettability map under the variable reservoir properties and conditions. We focus our  
 520 investigation on identifying the effects of the most impactful reservoir parameters on the oil-brine-  
 521 sandstone stability and wettability: pH, ionic strength, average rock site density and temperature  
 522 (as discussed in the previous sections). The evaluation range of each parameter is listed in Table 4.

523 The results of these analyses were combined and summarised as wettability maps as visualised in  
524 Figure 13 and Figure 14.

#### 525 *4.5.1 Wettability map for sandstone rock in NaCl*

526 Figure 13 shows the wettability map under the various combinations of reservoir properties and  
527 using NaCl as the background electrolyte in the brine. It depicts the reservoir conditions that result  
528 in negative MEB that indicates weak or intermediate wetting conditions. This map demonstrates  
529 the importance of salinity in determining reservoir wettability. Under almost all conditions,  
530 decreasing the brine salinity resulted in an increase in the strong water-wet conditions area in the  
531 map, especially, when the average rock site density is lower where the salinity effect is more  
532 pronounced. This demonstrates that the main focus of LSWF in sandstone reservoirs should involve  
533 reducing the brine ionic strength, which can result in shifting the reservoir wettability from  
534 weak/intermediate water-wet to strongly water-wet. Another important observation is the crucial  
535 role the average rock site density and clay mineralogy play in dictating the reservoir wettability.  
536 The map in Figure 13 shows that having a higher site density such as 5.5 site/nm<sup>2</sup> causes the  
537 reservoir to become weak water-wet over a wide range of reservoir conditions. This observation  
538 highlights the importance of rock mineralogy in terms of composition and clay content and  
539 appropriately modelling it in wettability predictions.

540 The wettability map also shows that the increase in temperature from 25 to 100 °C moves the  
541 reservoir wettability towards more wetting conditions within the studied range of parameters.  
542 Hence, indicating that hot low salinity waterflooding would be more beneficial under certain  
543 reservoir conditions.



544

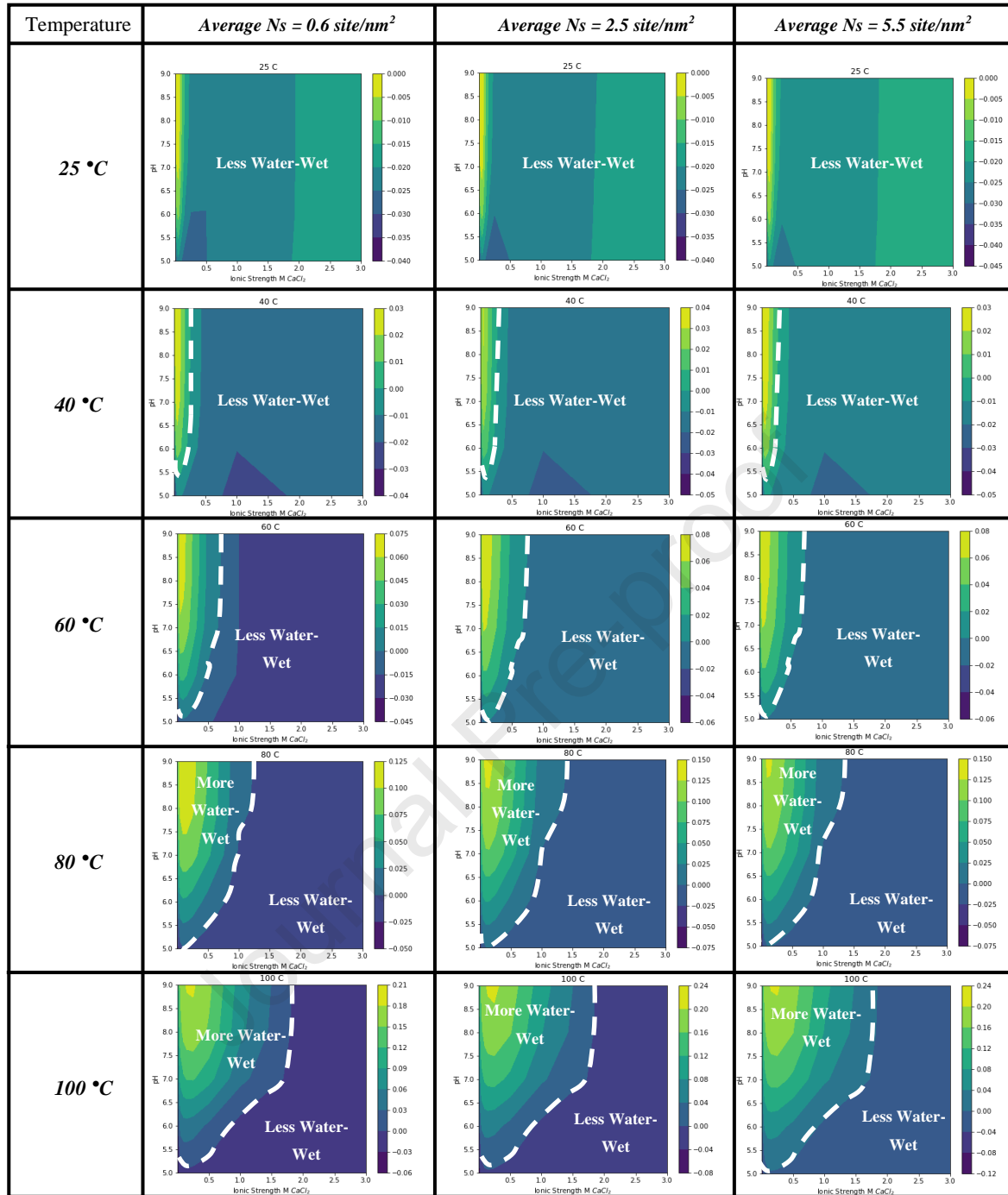
545 **Figure 13 Wettability map against NaCl ionic strength, pH, temperature, and average rock site**  
 546 **density**

#### 547 4.5.2 Wettability map for sandstone rock in $\text{CaCl}_2$

548 The same wettability map approach was used to evaluate the influence of the divalent cations such  
 549 as  $\text{Ca}^{2+}$  in the formation brine<sup>2</sup> on the reservoir wettability. The same ranges listed in Table 4 for

550 the rest of the reservoir parameters are used. The wettability map in Figure 14, demonstrates how  
551 impactful the presence of the calcium ion is on the reservoir wettability in comparison with the  
552 monovalent sodium ion (see Figure 13). The strong water-wet area in the adhesion map (Figure 14)  
553 increases as the pH and temperature values increase which enhance the deprotonation of surface  
554 sites leading to higher negative surface charge and repulsion between the two surfaces. The increase  
555 in the average rock surface site density from 0.6 to 5.5 site/nm<sup>2</sup> suppresses the strong water-wet  
556 area in the adhesion map. This can be attributed to the increase in the available surface sites for the  
557 positive Ca<sup>2+</sup> ions to adsorb on and screen the negative charge present at the rock surface.

558 Overall, the presence of the calcium ion significantly suppresses the areas of strong water  
559 wettability under different conditions. Such finding is directly linked with the way how the calcium  
560 ion affects the zeta potential at sandstone and oil-brine interfaces. Adsorption of Ca<sup>2+</sup> greatly  
561 reduces the negative values of the zeta potential and surface charge in comparison to sodium ion  
562 thereby resulting in less electrostatic repulsion between the two interfaces. As a result, significant  
563 low salinity effect and wettability alteration are expected if low salinity NaCl brine is injected into  
564 sandstone reservoirs comprising of calcium-rich formation water.



565

566

Figure 14 Wettability map against  $\text{CaCl}_2$  ionic strength, pH, temperature, and average rock site

567

density

568 **5 Summary and Conclusions**

569 A new sandstone-brine triple-layer surface complexation model was developed and validated

570 against results from the published experimental studies. The developed model is the first to

571 accommodate the individual and combined effects of sandstone minerals on the overall zeta

572 potential. The stability of the COBR system was analysed by calculating the disjoining pressure  
573 and interaction potential energy between the COBR interfaces using the DLVO. Furthermore, we  
574 introduced a new maximum energy barrier (MEB) concept as an indicator of reservoir wettability.  
575 The MEB was correlated well with contact angle measurements from the reported experimental  
576 studies. Analysis of the results showed that the contact angle value increases abruptly as the MEB  
577 drops below the zero-value indicating that the COBR system becomes unstable and less water-wet.  
578 This finding validates the application of maximum energy barrier concept (maximum of the  
579 interaction potential energy curve) to characterise reservoir wettability as a function of brine, oil  
580 and rock compositions, and reservoir conditions.

581 The developed TLM and MEB parameters were utilised to analyse the effect of sandstone  
582 mineralogy on the rock-brine zeta potential and reservoir wettability. The presence of kaolinite in  
583 the sandstone reservoir causes the COBR system to become less stable and less water-wet in  
584 comparison with the other studied clay minerals i.e. chlorite, illite, montmorillonite and smectite.  
585 Further sensitivity analysis indicated that the brine composition is the most impacting parameter  
586 on reservoir wettability amongst the investigated parameters. The importance of different studied  
587 parameters on reservoir wettability in sandstones was found to be in the following order: ionic  
588 strength and brine composition > pH > temperature > sandstone mineralogy > oil TAN > oil TBN.  
589 Furthermore, the rapid change in the maximum energy curve with the average rock site density  
590 demonstrates the significance of the sandstone rock mineralogy in dictating the wettability of the  
591 oil-brine-sandstone system. Also, the presence of  $\text{CaCl}_2$  in the formation water significantly  
592 suppresses the areas of strong water wettability under different reservoir conditions compared to  
593 NaCl.

594 The modelling work conducted in this research is limited to the types of clay considered in the  
595 sandstone-brine triple-layer model i.e. kaolinite, chlorite, illite, montmorillonite and smectite.  
596 Other clays and minerals may also be present in a sandstone rock. Moreover, the validation range

597 of the data used for optimising the developed oil-brine and sandstone-brine models is between 50  
 598 and 175,000 ppm for brine salinity, between 25 and 65 °C for temperatures and 2 – 11 pH. The  
 599 application of the developed workflow was also extended outside these validation ranges to gain  
 600 valuable insights into how these different parameters affect sandstone wettability. Nonetheless, the  
 601 workflow presented in this study will provide useful practical guidelines in screening sandstone  
 602 reservoir candidates for potential low salinity waterflooding applications.

## 603 **6 Abbreviations and Nomenclature**

### 604 **6.1 Abbreviations**

CD-MUSIC	Charge-distribution multisite surface complexation
COBR	Crude oil-brine-rock
DLVO	Derjaguin, Landau, Verwey, and Overbeek
LSE	Low salinity effect
LSWF	Low salinity waterflooding
MEB	Maximum energy barrier
MIE	Multicomponent ion exchange
PDI	Potential determining ions
SCM	Surface complexation modelling
TAN	Total acid number
TBN	Total base number
TLM	Triple-layer surface complexation models

VdW

Van der Waal

605

606 **6.2 Nomenclature**

A

Hamaker constant

 $A_{v=0}, A_{v>0}$ 

Contributions to Hamaker constant at zero and finite frequencies

 $A_s$ 

Structural force coefficient

 $C_1, C_2$ 

Capacitances of the inner and outer Helmholtz layers

 $d$ 

Thickness of the layer

 $e$ 

Electron charge

 $F$ 

Faraday constant

 $h$ 

Distance between the two interfaces

 $I$ 

Ionic strength of the solution

 $k_B$ 

Boltzmann constant

 $MW_{KOH}$ 

Molecular weight of KOH

 $n_1, n_2, n_3$ 

Refractive indexes for medium 1, 2, 3

 $N_A$ 

Avogadro's number

 $n_b$ 

Ion density in the bulk solution

 $N_s$ 

Surface site density

 $T$ 

Temperature

 $x$ 

Distance away from the surface in meters

 $\epsilon_0$ 

Dielectric constant of free space

 $\epsilon$ 

Relative dielectric constant

 $\zeta$ 

Zeta potential



$\kappa$	Debye-Huckel parameter
$\lambda_{lw}$	London wavelength
$\Pi(h)$	Disjoining pressure
$\Pi_{electric}(h)$	Electrostatic forces
$\Pi_{structural}(h)$	Structural forces
$\Pi_{vdw}(h)$	Van der Waals forces
$\rho$	Ionic concentration
$\sigma$	Charge density
$\psi$	Potential
$\psi_r$	Reduced surface potential

## 607 7 References

- 608 [1] J.J. Sheng, Critical review of low-salinity waterflooding, *Journal of Petroleum Science and*  
609 *Engineering*. 120 (2014) 216-224.
- 610 [2] S.C. Ayirala and A.A.Yousef, A state-of-the-art review to develop injection-water-chemistry  
611 requirement guidelines for IOR/EOR projects. *SPE Production & Operations*, 30(01),  
612 (2015)\_pp.26-42.
- 613 [3] S.O. Olayiwola and M. Dejam, A comprehensive review on interaction of nanoparticles with  
614 low salinity water and surfactant for enhanced oil recovery in sandstone and carbonate reservoirs.  
615 *Fuel*, 241, (2019) pp.1045-1057.
- 616 [4] S.O. Olayiwola and M. Dejam, Synergistic interaction of nanoparticles with low salinity water  
617 and surfactant during alternating injection into sandstone reservoirs to improve oil recovery and  
618 reduce formation damage. *Journal of Molecular Liquids*, 317, (2020) p.114228.
- 619 [5] S. Ayirala, A. AlSofi, Z. AlYousef, J. Wang, M.A. Alsaud and A. AlYousef, SmartWater based  
620 synergistic technologies for enhanced oil recovery. *Fuel*, 316, (2022) p.123264.
- 621 [6] D.J. Ligthelm, J. Gronsveld, J. Hofman, N. Brussee, F. Marcelis, H. van der Linde, Novel  
622 waterflooding strategy by manipulation of injection brine composition. (2009).
- 623 [7] P. McGuire, J. Chatham, F. Paskvan, D. Sommer, F. Carini, Low salinity oil recovery: An  
624 exciting new EOR opportunity for Alaska's North Slope, (2005).

- 625 [8] G. Tang, N.R. Morrow, Influence of brine composition and fines migration on crude  
626 oil/brine/rock interactions and oil recovery, *Journal of petroleum science and engineering*. 24  
627 (1999) 99-111.
- 628 [9] A. Lager, K.J. Webb, C. Black, M. Singleton, K.S. Sorbie, Low salinity oil recovery-an  
629 experimental investigation1, *Petrophysics-The SPWLA Journal of Formation Evaluation and*  
630 *Reservoir Description*. 49 (2008).
- 631 [10] J. Buckley, N. Morrow, Improved oil recovery by low salinity waterflooding: A mechanistic  
632 review, (2010) 6-9.
- 633 [11] R.A. Nasralla, H.A. Nasr-El-Din, Double-layer expansion: is it a primary mechanism of  
634 improved oil recovery by low-salinity waterflooding? *SPE Reservoir Evaluation & Engineering*.  
635 17 (2014) 49-59.
- 636 [12] A.N. Awolayo, H.K. Sarma, L.X. Nghiem, Brine-dependent recovery processes in carbonate  
637 and sandstone petroleum reservoirs: review of laboratory-field studies, interfacial mechanisms and  
638 modeling attempts. *Energies*, 11 (2018) p.3020.
- 639 [13] P.V. Brady, J.L. Krumhansl, A surface complexation model of oil–brine–sandstone interfaces  
640 at 100 C: Low salinity waterflooding, *Journal of Petroleum Science and Engineering*. 81 (2012)  
641 171-176.
- 642 [14] S. Erzuah, I. Fjelde, A.V. Omekeh, Wettability estimation by surface complexation  
643 simulations, (2017).
- 644 [15] Y. Elakneswaran, M. Shimokawara, T. Nawa, S. Takahashi, Surface complexation and  
645 equilibrium modelling for low salinity waterflooding in sandstone reservoirs, (2017).
- 646 [16] Q. Xie, F. Liu, Y. Chen, H. Yang, A. Saeedi, M.M. Hossain, Effect of electrical double layer  
647 and ion exchange on low salinity EOR in a pH controlled system, *Journal of Petroleum Science*  
648 *and Engineering*. 174 (2019) 418-424.
- 649 [17] Q. Xie, P.V. Brady, E. Pooryousefy, D. Zhou, Y. Liu, A. Saeedi, The low salinity effect at  
650 high temperatures, *Fuel*. 200 (2017) 419-426.
- 651 [18] R. Khaledialidusti, J. Kleppe, Surface-charge alteration at the carbonate/brine interface during  
652 single-well chemical-tracer tests: Surface-complexation model, *SPE Journal*. 23 (2018) 2302-2315.
- 653 [19] E. Pooryousefy, Q. Xie, Y. Chen, A. Sari, A. Saeedi, Drivers of low salinity effect in sandstone  
654 reservoirs, *Journal of Molecular Liquids*. 250 (2018) 396-403.
- 655 [20] H. Sharma, K.K. Mohanty, An experimental and modeling study to investigate brine-rock  
656 interactions during low salinity water flooding in carbonates, *Journal of Petroleum Science and*  
657 *Engineering*. 165 (2018) 1021-1039.
- 658 [21] Y. Chen, Q. Xie, A. Saeedi, Role of ion exchange, surface complexation, and albite dissolution  
659 in low salinity water flooding in sandstone, *Journal of Petroleum Science and Engineering*. 176  
660 (2019) 126-131.

- 661 [22] N. Kallay, D. Kovačević, S. Žalac, Thermodynamics of the solid/liquid interface-its  
662 application to adsorption and colloid stability, in: Anonymous Interface Science and Technology,  
663 Elsevier, 2006, pp. 133-170.
- 664 [23] A.R. Vieira, Surface Complexation Modeling of Lead (II), Cadmium (II) and Selenium (IV)  
665 Onto Iron Hydroxides in Single and Bisolute Systems, The University of Texas at Austin, 2006.
- 666 [24] M. Villalobos, Triple layer modelling of carbonate adsorption on goethites with variable  
667 adsorption capacities based on congruent site-occupancy, in: Anonymous Interface Science and  
668 Technology, Elsevier, 2006, pp. 417-442.
- 669 [25] M. Takeya, A. Ubaidah, M. Shimokawara, H. Okano, T. Nawa, Y. Elakneswaran, Crude  
670 oil/brine/rock interface in low salinity waterflooding: Experiments, triple-layer surface  
671 complexation model, and DLVO theory, Journal of Petroleum Science and Engineering. 188 (2020)  
672 106913.
- 673 [26] M. Takeya, M. Shimokawara, Y. Elakneswaran, H. Okano, T. Nawa, Effect of acid number  
674 on the electrokinetic properties of crude oil during low-salinity waterflooding, Energy Fuels. 33  
675 (2019) 4211-4218.
- 676 [27] F. Liu, M. Wang, Electrokinetic Mechanisms and Synergistic Effect on Ion-Tuned Wettability  
677 in Oil-Brine-Rock Systems, Transp. Porous Media. (2021) 1-20.
- 678 [28] M. Takeya, M. Shimokawara, Y. Elakneswaran, T. Nawa, S. Takahashi, Predicting the  
679 electrokinetic properties of the crude oil/brine interface for enhanced oil recovery in low salinity  
680 water flooding, Fuel. 235 (2019) 822-831.
- 681 [29] J.T. Tetteh, A. Pham, E. Peltier, J.M. Hutchison, R.B. Ghahfarokhi, Predicting the  
682 electrokinetic properties on an outcrop and reservoir composite carbonate surfaces in modified  
683 salinity brines using extended surface complexation models, Fuel. 309 (2022) 122078.
- 684 [30] M. Taheriotaghsara, M. Bonto, H.M. Nick, A.A. Eftekhari, Estimation of calcite wettability  
685 using surface forces, Journal of Industrial and Engineering Chemistry. 98 (2021) 444-457.
- 686 [31] M. Bonto, A.A. Eftekhari, H. M. Nick, Wettability Indicator Parameter Based on the  
687 Thermodynamic Modeling of Chalk-Oil-Brine Systems, Energy Fuels. 34 (2020) 8018-8036.
- 688 [32] P.V. Brady, N.R. Morrow, A. Fogden, V. Deniz, N. Loahardjo, Electrostatics and the low  
689 salinity effect in sandstone reservoirs, Energy Fuels. 29 (2015) 666-677.
- 690 [33] P. Leroy, A. Revil, A triple-layer model of the surface electrochemical properties of clay  
691 minerals, J. Colloid Interface Sci. 270 (2004) 371-380.
- 692 [34] O.L. Gaskova, M.B. Bukaty, Sorption of different cations onto clay minerals: modelling  
693 approach with ion exchange and surface complexation, Physics and Chemistry of the Earth, Parts  
694 A/B/C. 33 (2008) 1050-1055.
- 695 [35] M. Saeed, P. Jadhawar, Y. Zhou, R. Abhishek, Triple-Layer Surface Complexation Modelling:  
696 Characterization of Oil-Brine Interfacial Zeta Potential Under Varying Conditions of Temperature,

- 697 pH, Oil Properties and Potential Determining Ions, Colloids Surf. Physicochem. Eng. Aspects.  
698 (2022) 127903.
- 699 [36] A. Hurst, J. Archer, Sandstone reservoir description: An overview of the role of geology and  
700 mineralogy, Clay Miner. 21 (1986) 791-809.
- 701 [37] G. Hirasaki, Wettability: fundamentals and surface forces, SPE Form. Eval. 6 (1991) 217-226.
- 702 [38] N. Vdović, I. Jurina, S.D. Škapin, I. Sondi, The surface properties of clay minerals modified  
703 by intensive dry milling—revisited, Appl. Clay. Sci. 48 (2010) 575-580.
- 704 [39] Q. Du, Z. Sun, W. Forsling, H. Tang, Acid–base properties of aqueous illite surfaces, J. Colloid  
705 Interface Sci. 187 (1997) 221-231.
- 706 [40] E. Tertre, S. Castet, G. Berger, M. Loubet, E. Giffaut, Surface chemistry of kaolinite and Na-  
707 montmorillonite in aqueous electrolyte solutions at 25 and 60 C: Experimental and modeling study,  
708 Geochim. Cosmochim. Acta. 70 (2006) 4579-4599.
- 709 [41] J.M. Zachara, J.P. McKinley, Influence of hydrolysis on the sorption of metal cations by  
710 smectites: Importance of edge coordination reactions, Aquat. Sci. 55 (1993) 250-261.
- 711 [42] M. Hasegawa, M. Kimata, M. Shimane, T. Shoji, M. Tsuruta, The effect of liquid additives  
712 on dry ultrafine grinding of quartz, Powder Technol. 114 (2001) 145-151.
- 713 [43] P.W. Glover, E. Walker, M.D. Jackson, Streaming-potential coefficient of reservoir rock: A  
714 theoretical model, Geophysics. 77 (2012) D17-D43.
- 715 [44] J.N. Israelachvili, Intermolecular and Surface Forces, Academic press, 2015.
- 716 [45] D.L. Parkhurst, C. Appelo, Description of input and examples for PHREEQC version 3: a  
717 computer program for speciation, batch-reaction, one-dimensional transport, and inverse  
718 geochemical calculations. (2013).
- 719 [46] U. Farooq, M.T. Tweheyo, J. Sjöblom, G. Øye, Surface characterization of model, outcrop,  
720 and reservoir samples in low salinity aqueous solutions, J. Dispersion Sci. Technol. 32 (2011) 519-  
721 531.
- 722 [47] X. Quan, W. Jiazhong, Q. Jishun, L. Qingjie, M. Desheng, L. Li, L. Manli, Investigation of  
723 electrical surface charges and wettability alteration by ions matching waterflooding, (2012) 27-30.
- 724 [48] A. Bazyari, B.S. Soulgani, M. Jamialahmadi, A. Dehghan Monfared, A. Zeinijahromi,  
725 Performance of smart water in clay-rich sandstones: experimental and theoretical analysis, Energy  
726 Fuels. 32 (2018) 10354-10366.
- 727 [49] C. Chassagne, F. Mietta, J. Winterwerp, Electrokinetic study of kaolinite suspensions, J.  
728 Colloid Interface Sci. 336 (2009) 352-359.
- 729 [50] Q. Xie, Y. Liu, J. Wu, Q. Liu, Ions tuning water flooding experiments and interpretation by  
730 thermodynamics of wettability, Journal of Petroleum Science and Engineering. 124 (2014) 350-  
731 358.

- 732 [51] M.B. Alotaibi, R.A. Nasralla, H.A. Nasr-El-Din, Wettability studies using low-salinity water  
733 in sandstone reservoirs, *SPE Reservoir Evaluation & Engineering*. 14 (2011) 713-725.
- 734 [52] Y. Yukselen-Aksoy, A. Kaya, A study of factors affecting on the zeta potential of kaolinite  
735 and quartz powder, *Environmental Earth Sciences*. 62 (2011) 697-705.
- 736 [53] A. Kaya, A.H. Oren, Y. Yukselen, Settling behavior and zeta potential of kaolinite in aqueous  
737 media, (2003).
- 738 [54] W. Van Riemsdijk, T. Hiemstra, The CD-MUSIC model as a framework for interpreting ion  
739 adsorption on metal (hydr) oxide surfaces, in: *Anonymous Interface Science and Technology*,  
740 Elsevier, 2006, pp. 251-268.
- 741 [55] J. Gregory, Approximate expressions for retarded van der Waals interaction, *J. Colloid  
742 Interface Sci.* 83 (1981) 138-145.
- 743 [56] R.J. Hunter, L.R. White, D.Y.C. Chan, *Foundations of Colloid Science*, Clarendon Press,  
744 1987.
- 745 [57] J. Buckley, K. Takamura, N. Morrow, Influence of electrical surface charges on the wetting  
746 properties of crude oils, *SPE reservoir engineering*. 4 (1989) 332-340.
- 747 [58] M. Sadeqi-Moqadam, S. Riahi, A. Bahramian, An investigation into the electrical behavior of  
748 oil/water/reservoir rock interfaces: The implication for improvement in wettability prediction,  
749 *Colloids Surf. Physicochem. Eng. Aspects*. 490 (2016) 268-282.
- 750 [59] H. Reerink, J.T.G. Overbeek, The rate of coagulation as a measure of the stability of silver  
751 iodide sols, *Discuss. Faraday Soc.* 18 (1954) 74-84.
- 752 [60] E.V. Lebedeva, A. Fogden, Adhesion of oil to kaolinite in water, *Environ. Sci. Technol.* 44  
753 (2010) 9470-9475.
- 754 [61] J.V. Nicolini, H.C. Ferraz, C.P. Borges, Effect of seawater ionic composition modified by  
755 nanofiltration on enhanced oil recovery in Berea sandstone, *Fuel*. 203 (2017) 222-232.
- 756 [62] H. Mahani, S. Berg, D. Ilic, W. Bartels, V. Joekar-Niasar, Kinetics of the low salinity  
757 waterflooding effect studied in a model system, (2013).
- 758 [63] I. Sondi, J. Bišćan, V. Pravdić, Electrokinetics of pure clay minerals revisited, *J. Colloid  
759 Interface Sci.* 178 (1996) 514-522.
- 760 [64] R.A. Nasralla, H.A. Nasr-El-Din, Impact of cation type and concentration in injected brine on  
761 oil recovery in sandstone reservoirs, *Journal of Petroleum Science and Engineering*. 122 (2014)  
762 384-395.
- 763 [65] A.A. da Costa, J. Soares, P. Rocha, G. Costa, M. Embiruçu, An experimental evaluation of  
764 low salinity water mechanisms in a typical Brazilian sandstone and light crude oil with low  
765 acid/basic number, *Fuel*. 273 (2020) 117694.

- 766 [66] A. Borysenko, B. Clennell, R. Sedev, I. Burgar, J. Ralston, M. Raven, D. Dewhurst, K. Liu,  
767 Experimental investigations of the wettability of clays and shales, Journal of Geophysical  
768 Research: Solid Earth. 114 (2009).
- 769 [67] Z.Y. Wang, P. Zhang, Z. Ma, On the physics of both surface overcharging and charge  
770 reversal at heterophase interfaces. Physical Chemistry Chemical Physics, 20(6) (2018), pp.4118-  
771 4128.

Journal Pre-proof

**Manuscript title:**

**Modelling the effects of reservoir parameters and rock mineralogy on wettability during low salinity waterflooding in sandstone reservoirs**

**Highlights:**

- Developed a triple-layer surface complexation model (TLM) to describe sandstone-brine interactions.
- Model validated using published experimental studies with accuracy between 78% and 90%.
- The maximum energy barrier (MEB) is proposed to characterise reservoir wettability as a novel concept.
- Investigated the most impactful parameters on sandstone reservoir wettability.
- Sandstone reservoirs with higher content of kaolinite will lead the wettability to become less water wet

**Declaration of interests**

The authors declare that they have no known competing financial interests or personal relationships that could have appeared to influence the work reported in this paper.

The authors declare the following financial interests/personal relationships which may be considered as potential competing interests:

Journal Pre-proof